Title
Multidecadal fluctuations of the North Atlantic Ocean and feedback on the winter climate in CMIP5 control simulations

Journal
Journal of Geophysical Research: Atmospheres, 121(6)

ISSN
2169-897X

Authors
Peings, Yannick
Simpkins, Graham
Magnusdottir, Gudrun

Publication Date
2016-03-27

DOI
10.1002/2015jd024107

AGU PUBLICATIONS

JGR

Journal of Geophysical Research: Atmospheres

RESEARCH ARTICLE
10.1002/2015JD024107

Key Points:
- Although large uncertainties in observations, the CMIP5 models seem to lack internally generated AMV
- Multiannual persistence of the wintertime NAO is a driver of the AMV, but no consistent feedback of the AMV onto the atmosphere is found
- A lagged NAO signal is identified in the two models that exhibit a large AMV

Supporting Information:
- Figures S1–S9

Correspondence to:
Y. Peings,
ypeings@uci.edu

Citation:
Peings, Y., G. Simpkins, and G. Magnusdottir (2016), Multidecadal fluctuations of the North Atlantic Ocean and feedback on the winter climate in CMIP5 control simulations, *J. Geophys. Res. Atmos.*, *120*, doi:10.1002/2015JD024107.

Received 18 AUG 2015
Accepted 24 FEB 2016
Accepted article online 29 FEB 2016

Multidecadal fluctuations of the North Atlantic Ocean and feedback on the winter climate in CMIP5 control simulations

Yannick Peings[1], Graham Simpkins[1], and Gudrun Magnusdottir[1]

[1]Department of Earth System Science, University of California, Irvine, California, USA

Abstract This study examines the relationship between the Atlantic Multidecadal Variability (AMV) and the wintertime atmospheric circulation of the North Atlantic in simulations of the fifth Coupled Model Intercomparison Project (CMIP5). Comparisons of internal (using preindustrial control simulations) and externally forced (using historical and Representative Concentration Pathways 8.5 simulations) simulated AMV with observations suggest that the CMIP5 models lack internally generated AMV, except for two models (GFDL-ESM2G and HadGEM2-ES). A long-term influence of the winter North Atlantic Oscillation (NAO) on the AMV is identified, but no consistent feedback of the AMV onto the atmospheric circulation is found among the models. However, GFDL-ESM2G and HadGEM2-ES show a small lagged NAO signal that suggests a driving role of the ocean on decadal fluctuations of the atmosphere, with two different potential mechanisms. HadGEM2-ES exhibits a latitudinal shift of the Atlantic Intertropical Convergence Zone that can modulate the NAO through a Rossby wave train emanating from the tropics. In GFDL-ESM2G, the AMV is associated with a decrease in storm track activity and a shift of the intraseasonal weather regimes toward the negative NAO regime. These results raise hope that some long-term predictability of the winter climate over the North Atlantic and surrounding continents could be extracted from long-term oceanic fluctuations of the North Atlantic Ocean, provided that the AMV is correctly represented in coupled ocean-atmosphere models.

1. Introduction

Climate variability occurs on all time scales, driven by either internal fluctuations of the climate system [e.g., *DelSole et al.*, 2011] or by external forcings such as volcanoes, variations in solar insolation, and greenhouse gas/aerosol concentrations [e.g., *Lean and Rind*, 2008]. North Atlantic sea surface temperature (SST) exhibits large multidecadal variability known as Atlantic Multidecadal Variability (AMV) [e.g., *Ting et al.*, 2011] or the Atlantic Multidecadal Oscillation [*Kerr*, 2000; *Enfield et al.*, 2001; *Knight et al.*, 2005]. From the late nineteenth century to present, North Atlantic SST has oscillated between a warm and a cold state with a period of about 60–70 years. The AMV is also present in paleoclimatic reconstructions, suggesting that the AMV is not a true oscillation but rather the manifestation of some persistence in the North Atlantic SST anomalies at the multidecadal time scale [e.g., *Gray et al.*, 2004; *Knudsen et al.*, 2011].

The causes of AMV remain unclear but have been related to both internal variability of the climate system as well as to natural and anthropogenic external forcings [e.g., *Ting et al.*, 2009; *Otterå et al.*, 2010; *Booth et al.*, 2012; *Terray*, 2012; *Knudsen et al.*, 2014; *Tandon and Kushner*, 2015]. Preindustrial climate simulations from general circulation models (GCMs) support the view that the AMV is generated by internal variations of the ocean [*Delworth and Mann*, 2000; *Knight et al.*, 2005; *Ting et al.*, 2014]. GCMs suggest that the AMV is tied to the Atlantic Meridional Overturning Circulation (AMOC) [e.g., *Delworth et al.*, 1993; *Muir and Fedorov*, 2015], although the observational record of the AMOC is too short to examine its long-term variability [*Cunningham et al.*, 2007]. The AMOC is the Atlantic component of the global thermohaline circulation, which is driven by temperature and salinity gradients in the ocean that modulate deep convection in high latitudes [e.g., *Kuhlbrodt et al.*, 2007]. Some climate simulations have suggested that the strength of the AMOC is modulated by low-frequency stochastic atmospheric variability and associated surface wind stress. In particular, a reinforcement of the AMOC is generally preceded by a persistent positive North Atlantic Oscillation (NAO) in winter [e.g., *Eden and Willebrand*, 2001; *Medhaug et al.*, 2012; *Barrier et al.*, 2014]. The NAO is the first mode of atmospheric variability in the Atlantic region in winter [*Hurrell and van Loon*, 1997]. Persistent anomalies in the NAO force some wind stress and heat flux anomalies that amplify or weaken the formation of the North Atlantic Deep Water masses [e.g., *Bersch*, 2002], which in turn leads to a reinforcement or

weakening of the AMOC with a couple of years lag (e.g., *Medhaug and Furevik*, 2011; *Yeager and Danabasoglu*, 2014). In several climate models, a reinforcement of the AMOC is then followed by a warming of the subpolar gyre and a buildup of the positive phase of the AMV (and conversely with a reduced AMOC) [*Zhang and Wang*, 2013]. However, the AMOC-AMV relationship differs in other models, either in the sign of the anomalies or in the timing of maximum correlation. *Tandon and Kushner* [2015] suggest that this discrepancy between models is due to the influence of external factors that have to be properly removed to isolate the internal component of the AMOC-AMV relationship. Although decadal predictability of AMV may be limited after removing the influence of external factors [*Tandon and Kushner*, 2015], the slow oceanic fluctuations represent the main source of predictability of the climate at decadal to multidecadal time scales [*Meehl et al*., 2014], especially for predicting SST, sea ice, and oceanic heat content in the subpolar North Atlantic gyre [*Keenlyside et al*., 2008; *Msadek et al*., 2010; *Yeager et al*., 2012; *Msadek et al*., 2014; *Yeager et al*., 2015]. More predictability would arise from the internal fluctuations of the North Atlantic Ocean if the oceanic anomalies in turn exert a significant feedback onto the atmospheric circulation. The determination of the feedback that AMV-related oceanic anomalies exert onto the atmosphere is the scope of the present study.

In his pioneering work, *Bjerknes* [1964] hypothesized that the atmosphere generally drives the ocean on short time scales (hourly to interannual) over the midlatitude North Atlantic Ocean (although this is not always the case, for example, in western boundary currents [*Minobe et al*., 2008]), while the ocean drives the atmosphere on longer periods (decadal to multidecadal). His hypothesis has been successfully verified using observations and reanalyses [*Cayan*, 1992; *Kushnir*, 1994; *Yu et al*., 2011] and/or coupled ocean-atmosphere climate simulations [*Visbeck et al*., 1998; *Rodwell and Folland*, 2002; *Woollings et al*., 2015]. The specific link between midlatitudinal North Atlantic SST and heat flux variability has been recently revisited by *Gulev et al.* [2013] using a reconstruction of turbulent heat fluxes over the twentieth century. In the Gulf Stream region, SST is negatively correlated with the heat flux anomalies at short time scales (under 10 years). This is consistent with the atmosphere driving short-term variations in heat flux exchange at the air-sea interface. Indeed, negative correlations indicate that more upward heat flux are associated with cooler SST, which is the relationship expected from the atmosphere driving the oceanic surface through surface wind stress. At longer time scales (more than 10 years), correlations are mainly positive (warmer SST is associated with upward heat flux anomalies), suggesting that heat flux anomalies are driven by the AMV and associated oceanic heat transport and convergence. This long-term SST-heat flux relationship indicates that slow fluctuations of the North Atlantic Ocean may have the potential to drive the climate of surrounding continents, giving perspective for long-range predictability.

The nature of climate patterns associated with the AMOC/AMV has been explored in numerous studies. Analyses of the AMV-NAO relationship in observations/reanalyses suggest that the warm (cold) AMV has preferentially coincided with periods of negative (positive) trends in the wintertime NAO [*Omrani et al*., 2014; *Peings and Magnusdottir*, 2014; *Gastineau and Frankignoul*, 2015]. However, the robustness of this inverse relationship between AMV and the NAO is uncertain due to the shortness of the observational record. Numerical experiments have also been used to investigate the response of the atmosphere to the AMV by prescribing SST anomalies to atmospheric GCMs (AGCMs). Results suggest that the AMV exerts a significant influence on various climate phenomena in summer, such as Atlantic hurricanes and Sahel monsoon rainfall [e.g., *Zhang and Delworth*, 2006; *Knight et al*., 2006]. In winter, the response of the atmosphere is less consistent and more model dependent [*Hodson et al*., 2010]. Nevertheless, several recent studies have shown that the positive AMV promotes the negative NAO in winter [*Msadek et al*., 2011; *Peings and Magnusdottir*, 2014; *Peings and Magnusdottir*, 2015, *Davini et al*. 2015]. *Omrani et al.* [2014] have compared the atmospheric response to the AMV in both a standard low-top version and a high-top version of their model that better resolves the stratosphere. They found a larger negative NAO response in the high-top model due to a significant perturbation of the polar stratospheric vortex by AMV-driven upward propagation of planetary waves. In their experiments, the polar vortex perturbation results in northern annular mode anomalies that propagate downward through troposphere-stratosphere interactions and project onto the NAO at the surface. On the other hand, numerical experiments from *Peings and Magnusdottir* [2015] and *Davini et al.* [2015] suggest that such a stratospheric response is not critical for simulating a significant modulation of the NAO. Indeed, the NAO response predominantly arises from tropical SST anomalies in their experiments, through a perturbation of tropical Atlantic precipitation and deep convection that forces a Rossby wave train into the extratropics. The response is then amplified by changes in baroclinicity and eddy-mean flow interactions that are induced by the extratropical component of the AMV-SST anomalies [*Peings and Magnusdottir*, 2015]. In short, the recent literature suggests

that the AMV might be one of the drivers of multidecadal fluctuations in the NAO. For instance, the positive trend of the NAO that was observed in the 1990s and the recent reversal toward negative values in winter [*Cohen et al*., 2014] could have been partly driven by the shift of the AMV toward its positive polarity at the end of the 1990s. Nevertheless, atmosphere-only modeling experiments are limited by the fact that they neglect some of the ocean-atmosphere interactions since SST is prescribed and thus noninteractive [*Chen et al*., 2013; *Chen and Schneider*, 2014]. Experiments have been performed with a slab-ocean model to consider ocean-atmosphere feedbacks in turbulent and radiative fluxes [*Msadek et al*., 2011; *Peings and Magnusdottir*, 2015], but they still neglect the ocean dynamics. In order to assess the importance of the full ocean-atmosphere coupling, *Omrani et al*. [2015] have compared the AMV-NAO relationship in coupled and uncoupled versions of their model and found substantial differences, despite a good agreement on the global characteristics of the atmospheric response. The wintertime atmospheric response to the AMV in the presence of a full ocean-atmosphere coupling is therefore still uncertain and has to be investigated in different GCMs to confirm that they support results from AGCMs experiments and observational analyses.

In this study, we explore ocean-atmosphere interactions of the North Atlantic basin in a set of preindustrial control simulations of the fifth Coupled Multimodel Intercomparison Project (CMIP5). These coupled ocean-atmosphere simulations are adapted for studying internal variability of the ocean-atmosphere system since they do not include any external forcing and are long enough to ensure robustness of statistical analyses. This work is complementary to previous studies that have investigated the AMV-NAO relationship in atmosphere-only simulations. Our objective is to determine whether the CMIP5 GCMs simulate a discernible influence of the AMV on the atmospheric circulation in winter, supporting the notion that there is potential predictability of the winter climate associated with the AMV. Section 2 presents the set of simulations and the statistical tools that are used in the study. Section 3 describes the nature of the AMV in the models then determines its linkage with the atmospheric circulation in winter with an emphasis on the NAO. A detailed analysis of a single model that exhibits some interesting results is then carried out. Finally, results are summarized and discussed in the conclusion section.

2. Data and Methods

2.1. CMIP5 Simulations and Observed Data

Twenty-three preindustrial control simulations (piControl) of the CMIP5 database have been selected based on the availability of monthly outputs for sea surface temperature, turbulent heat flux (sensible + latent), sea level pressure, and sea ice concentration fields. Only the control runs that include at least 500 years of data for these variables have been retained. Table 1 gives a list of the models with their abbreviations and their respective temporal coverage and spatial resolution. Seventeen modeling groups from all around the world are represented in this list. Details on the different models and experiments are available on the Program for Climate Model Diagnosis and Intercomparison portal (http://cmip-pcmdi.llnl.gov/cmip5/). Unlike historical or Representative Concentration Pathways (RCPs) simulations, external forcings (solar input and greenhouse gases/aerosols concentrations) are constant in preindustrial simulations through the course of the run. These simulations therefore represent internal variability of the climate system as simulated by the model independent of any external forcing. Twenty historical and RCP8.5 runs have also been concatenated and are used to briefly discuss the AMV and its relationship with the NAO in the presence of external forcing. These 20 models are the same models as for the piControl simulations except for BNU-ESM, MIROC5, and MPI-ESM-P for which the data were not available. For ease of comparison, all model outputs have been interpolated to a common $1.9° \times 2.5°$ regular grid and to 17 pressure levels for 4-D fields (from 1000 hPa to 10 hPa).

Concerning the observed data, sea surface temperature and sea ice concentration (SIC) come from the HadISST data set [*Rayner et al*., 2003], available over 1870–2013. Sea level pressure (SLP) comes from the 20th Century Reanalysis (20CR) [*Compo et al*., 2011] over 1871–2010. Finally, we also use the reconstruction of turbulent heat flux (sensible + latent) that is made available in the supporting information of *Gulev et al*. [2013]. The methodology that is used to reconstruct the turbulent fluxes is detailed in their Methods section and so are specifics of uncertainty in the data.

2.2. Definition of the Indices

2.2.1. AMV Indices

The AMV describes multidecadal fluctuations of the North Atlantic SST that are both internally generated and forced by external forcings such as greenhouse gases, aerosols, and volcanoes [e.g., *Knight*, 2009;

Table 1. List of CMIP Models and Length of Associated piControl Simulations

Acronym	Research Center	Years	AGCM Resolution
ACCESS1-0	Commonwealth Scientific and Industrial Research Organisation, and Bureau of Meteorology, Australia	500	1.875° × 1.25°, L38
ACCESS1-3	Commonwealth Scientific and Industrial Research Organisation, and Bureau of Meteorology, Australia	500	1.875° × 1.25°, L38
bcc-csm1-1	Beijing Climate Center, China	500	2.81° × 2.79°, L26
BNU-ESM	College of Global Change and Earth System Science, Beijing Normal University, China	559	2.81° × 2.79°, L26
CanESM2	Canadian Center for Climate Modeling and Analysis, Canada	996	2.81° × 2.79°, L35
CCSM4	National Center for Atmospheric Research, USA	501	1.25° × 0.90°, L26
CESM1-BGC	National Center for Atmospheric Research, USA	500	1.25° × 0.90°, L26
CMCC-CMS	Centro Euro-Mediterraneo per I Cambiamenti Climatici, Italy	500	1.875° × 1.865°, L95
CNRM-CM5	Centre National de Recherches Meteorologiques/Centre Europeen de Recherche et Formation Avancees en Calcul Scientifique, France	850	1.41° × 1.40°, L31
CSIRO-Mk3-6-0	Commonwealth Scientific and Industrial Research Organisation, in collaboration with the Queensland Climate Change Centre of Excellence, Australia	500	1.875° × 1.865°, L18
FIO-ESM	The First Institute of Oceanography, China	800	2.8° × 2.8°, L26
GFDL-ESM2G	U.S. Department of Commerce/National Oceanic and Atmospheric Administration/Geophysical Fluid Dynamics Laboratory, USA	500	2.50° × 2°, L24
GFDL-ESM2M	U.S. Department of Commerce/National Oceanic and Atmospheric Administration/Geophysical Fluid Dynamics Laboratory, USA	500	2.50° × 2°, L24
GISS-E2-H	National Aeronautics and Space Administration/Goddard Institute for Space Studies, USA	540	2.50° × 2°, L40
GISS-E2-R	National Aeronautics and Space Administration/Goddard Institute for Space Studies, USA	850	2.50° × 2°, L40
HadGEM2-ES	Met office Hadley Centre, UK	576	1.875° × 1.25°, L38
inmcm4	Institute for Numerical Mathematics, Russia	500	2° × 1.50°, L21
MIROC5	Center for Climate System Research (University of Tokyo), National Institute for Environmental Studies, and Frontier Research Center for Global Change, Japan	670	1.41° × 1.40°, L40
MPI-ESM-LR	Max Planck Institute for Meteorology, Germany	1000	1.875° × 1.875°, L47
MPI-ESM-MR	Max Planck Institute for Meteorology, Germany	1000	1.875° × 1.875°, L95
MPI-ESM-P	Max Planck Institute for Meteorology, Germany	1156	1.875° × 1.875°, L47
MRI-CGCM3	Meteorological Research Institute, Japan	500	1.125° × 1.12°, L48
NorESM1-M	Norwegian Climate Centre, Norway	501	2.50° × 1.895°, L26

Knudsen et al., 2014; *Ting et al.*, 2014; *Tandon and Kushner*, 2015]. Differentiating the internal component from the externally forced component of the observed AMV is a challenge that has to be addressed before comparing observations with CMIP5 simulations.

No external forcings are included in the piControl simulations, such that the AMV from these runs represents the internal component of AMV as simulated by the CMIP5 models. The AMV index from these runs is defined as the annual average of detrended North Atlantic SST anomalies (80°W/10°E; 0/70°N). The detrending is applied to remove any possible drift in the simulations (note that this detrending is applied to all indices and anomaly fields from the piControl simulations). As for each AMV index that is used in this study, a Lanczos filter is applied to the time series in order to separate the low-frequency fluctuations of the North Atlantic SST from the high-frequency fluctuations (low-pass filter with a cutoff frequency of 10 years).

For observations, different methods exist to isolate the internal component of the AMV from the forced SST variability due to external forcings [*Knight*, 2009]. The simplest method consists of removing a linear trend from the North Atlantic SST anomalies [*Enfield et al.*, 2001]. However, the SST warming is nonlinear, and a simple detrending does not remove the AMV fluctuations that arise from multidecadal variability in external forcings [*Terray*, 2012; *Tandon and Kushner*, 2015]. An alternative method suggested by *Trenberth and Shea* [2006] is to remove global mean SST anomalies, which are highly correlated with nonlinear variations in external forcing [*Ting et al.*, 2009], from North Atlantic SST anomalies prior to computing the AMV index. A limitation of this method is that global mean SST anomalies include part of the North Atlantic signal, such that subtracting them can lead to partial cancelation of the AMV signal. Moreover, it does not directly account for regional variations in external forcings, such as volcanic eruptions or anthropogenic aerosols that exert a local influence on the

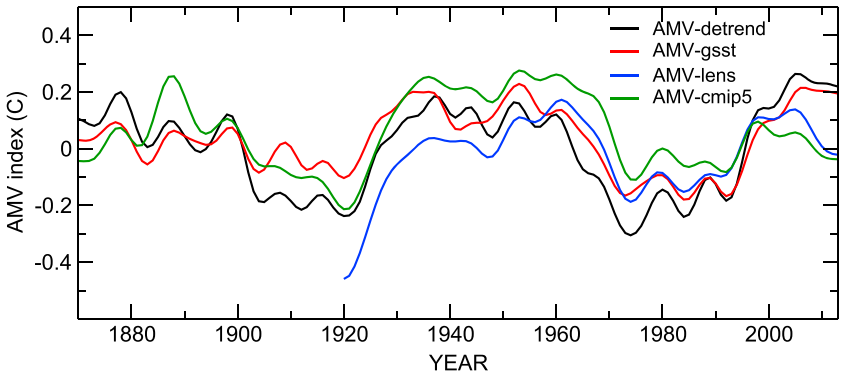

Figure 1. Comparison of the observed AMV index over 1870–2013 using different methods for removing the forced component of North Atlantic SST: linear detrending of the North Atlantic SST anomalies (AMV-detrend, black), removal of global SST anomalies (AMV-gsst, red), removal of the ensemble mean of North Atlantic SST as simulated in 40 members of the CESM-LENS simulations (1920–2013, AMV-lens, blue), removal of the ensemble mean of North Atlantic SST as simulated in 20 historical/RCP8.5 CMIP5 simulations (AMV-cmip5, green).

North Atlantic SST [*Otterå et al.*, 2010]. In order to directly estimate the externally forced component of the North Atlantic SST, a hybrid approach has been developed that uses the ensemble mean of GCM simulations to estimate the forced component of North Atlantic SST. Averaging a large ensemble of historical/RCP simulations retains only the forced component of the North Atlantic SST and removes internal variability. This forced component, estimated from GCMs, is then subtracted from the observed North Atlantic SST to isolate fluctuations that are due to internal processes only [*Knight*, 2009; *Ting et al.*, 2014; *Tandon and Kushner*, 2015]. Using an ensemble mean of simulations has the advantage of being an independent estimate of the externally forced component of the AMV, with the caveat of mixing observational with model results and thus being contaminated by possible biases in the GCMs sensitivity to external forcings in the North Atlantic. Since each method has its limitations, we have computed three different indices representing the internal AMV in observations, which allow us to discuss uncertainties when comparing observations to the piControl simulations. **AMV-gsst** follows the method of *Trenberth and Shea* [2006], by subtracting global mean SST anomalies from North Atlantic SST anomalies. The SST anomalies are relative to the 1981–2010 climatology, and a Lanczos low-pass filter retains only low-frequency fluctuations (>10 years). **AMV-cmip5** uses the ensemble mean of the 20 historical/RCP8.5 simulations to estimate the forced component of the North Atlantic SST. Due to the relatively large ensemble size, the ensemble mean of North Atlantic SST over the observational period (1870–2013) gives a good estimate of the forced component of the North Atlantic SST variability, which is subtracted from the observed AMV to retain the unforced AMV only. **AMV-lens** follows the same methodology as AMV-cmip5, but the forced component of North Atlantic SST is estimated from the ensemble mean of the Community Earth System Model large ensemble of simulations (CESM-LENS) [*Kay et al.* 2015]. To date, 40 members of coupled ocean-atmosphere simulations over the 1920–2100 period have been performed with observed and estimated external forcings from the RCP8.5 scenario. AMV-lens therefore spans the 1920–2013 period.

A fourth AMV index is used, **AMV-detrend**, which is computed from detrended North Atlantic SST anomalies. As discussed before, this index includes the externally forced multidecadal fluctuations of the AMV, especially due to multidecadal variations in volcanic and anthropogenic aerosol forcings. This index is thus compared to similarly detrended AMV indices from the historical/RCP8.5 simulations, allowing us to determine whether some of our observations versus models comparisons differ when multidecadal variability in external forcings is present in the time series.

The four observed AMV indices are shown in Figure 1 over the 1870–2013 period (1920–2013 for AMV-lens). The indices agree on the presence of a warm period between the 1930s and 1970s, with colder conditions before 1930 and between the 1970s and the mid-1990s. However, there is less consistency concerning the amplitude of the recent warm period that is less pronounced in AMV-lens and AMV-cmip5, suggesting that the two other methods underestimate the forced component of North Atlantic SST in recent decades, in line with *Tandon and Kushner* [2015] and *Steinman et al.* [2015]. Henceforth, we select AMV-gsst as our best estimate of internal AMV in observations since it is observation-based only, and its spatial pattern exhibits larger consistency with the

Table 2. Spatial Correlation and Root-Mean-Square Error (RMSE) in °C Between the Pattern of AMV in piControl Simulations and the Observed Pattern of AMV (Derived From, Respectively, AMV-gsst, AMV-cmip5, and AMV-lens)[a]

Model	Spatial *R*	RMSE (°C)	Variance Ratio (%) (10–140 Year window)[a]	Persistence (observation: 10/12/7 year)[b]
ACCESS1-0	0.59/0.31/0.49	0.13/0.16/0.15	88/78/73	5
ACCESS1-3	0.51/0.25/0.42	0.19/0.21/0.20	82/73/66	4
bcc-csm1	0.34/0.33/0.35	0.18/0.17/0.17	68/61/58	4
BNU-ESM	0.72/0.44/0.59	0.11/0.14/0.12	63/57/52	5
CanESM2	0.59/0.34/0.50	0.10/0.09/0.08	64/57/53	5
CCSM4	0.51/0.29/0.44	0.11/0.09/0.08	50/42/41	5
CESM1-BGC	0.56/0.27/0.46	0.12/0.11/0.10	44/40/36	4
CMCC-CMS	0.59/0.32/0.40	0.12/0.13/0.13	76/68/62	6
CNRM-CM5	0.66/0.25/0.47	0.11/0.15/0.13	72/64/52	6
CSIRO-Mk3-6-0	0.67/0.43/0.58	0.17/0.21/0.19	66/59/52	6
FIO-ESM	0.75/0.35/0.58	0.09/0.11/0.09	55/49/44	5
GFDL-ESM2G	0.76/0.40/0.61	0.22/0.27/0.25	118/105/96	7
GFDL-ESM2M	0.62/0.21/0.44	0.11/0.14/0.12	74/66/58	5
GISS-E2-H	0.65/0.32/0.51	0.12/0.08/0.08	43/38/35	4
GISS-E2-R	0.71/0.29/0.50	0.11/0.10/0.10	57/51/44	6
HadGEM2-ES	0.66/0.43/0.63	0.17/0.22/0.20	113/101/87	7
INMCM4	0.69/0.34/0.58	0.15/0.20/0.18	82/73/67	5
MIROC5	0.68/0.28/0.51	0.22/0.27/0.24	78/70/64	5
MPI-ESM-LR	0.55/0.27/0.41	0.12/0.14/0.13	80/72/65	5
MPI-ESM-MR	0.47/0.23/0.33	0.13/0.14/0.14	79/71/66	5
MPI-ESM-P	0.53/0.24/0.36	0.11/0.13/0.12	83/74/68	5
MRI-CGCM3	0.42/0.38/0.43	0.15/0.15/0.14	59/53/47	5
NorESM1-M	0.42/0.40/0.48	0.12/0.07/0.08	54/48/45	4

[a]A Ratio of North Atlantic SST variance in piControl simulations compared to observations (in %). For models a band-pass filter is applied to remove variability outside of the 10-144 year window of the observed AMV (10-94 year window when compared to AMV-lens).
[b]Persistence of the AMV in piControl simulations, based on the *e*-folding time of autocorrelation of the AMV time series.

AMV pattern from piControl simulations than other methods (Table 2 and discussion in section 3.1). However, uncertainties related to the choice of the observed AMV index are discussed throughout the paper.

2.2.2. Other Indices

The NAO index is defined as the first mode of an empirical orthogonal function (EOF) analysis applied to the wintertime (December to March, DJFM) sea level pressure in the North Atlantic/Europe sector (85°W/60°E; 20°N/90°N). The high-frequency fluctuations are removed from the NAO index using the same Lanczos filter as for the AMO index, this NAO index is referred to as the decadal NAO index.

The AMOC index is derived from the maximum value of the Atlantic meridional overturning circulation in the 500–5000 m oceanic column and between the latitude range 20–40°N. The meridional overturning circulation is derived from an integration of the meridional velocity of the Atlantic Ocean. Monthly values are then averaged annually to obtain a yearly index of the AMOC, and the same Lanczos filter as for the AMO index is applied to the time series to remove interannual variability and construct a decadal AMOC index.

2.3. Statistical Tools

Correlations and composites are used to explore the relationship between the various climate parameters of interest. The statistical significance of correlations is determined using a phase-scrambled bootstrap method [*Davison and Hinkley*, 1997] that accounts for autocorrelation in the time series (1000 iterations). Composites are computed by differentiating years with high values of the AMV from years with low values, based on upper and lower quartile thresholds. The statistical significance of composite analyses is determined using a bootstrap method with 1000 iterations of randomly selected composite years (at each grid point the *p* value gives the fraction of random composites that exhibit a larger value than the original composite). Agreement between models is considered high when at least 75% agree on the sign of the composite anomaly or correlation (i.e., at least 18 out of 23).

The North Atlantic weather regimes discussed in section 3.4 are computed using a *k* mean clustering algorithm applied to the daily anomalies of the 500 hPa geopotential height (Z500) [*Michelangeli et al.*, 1995]. Four centroids are retained by this algorithm, then each day is attributed to one of these centroids according

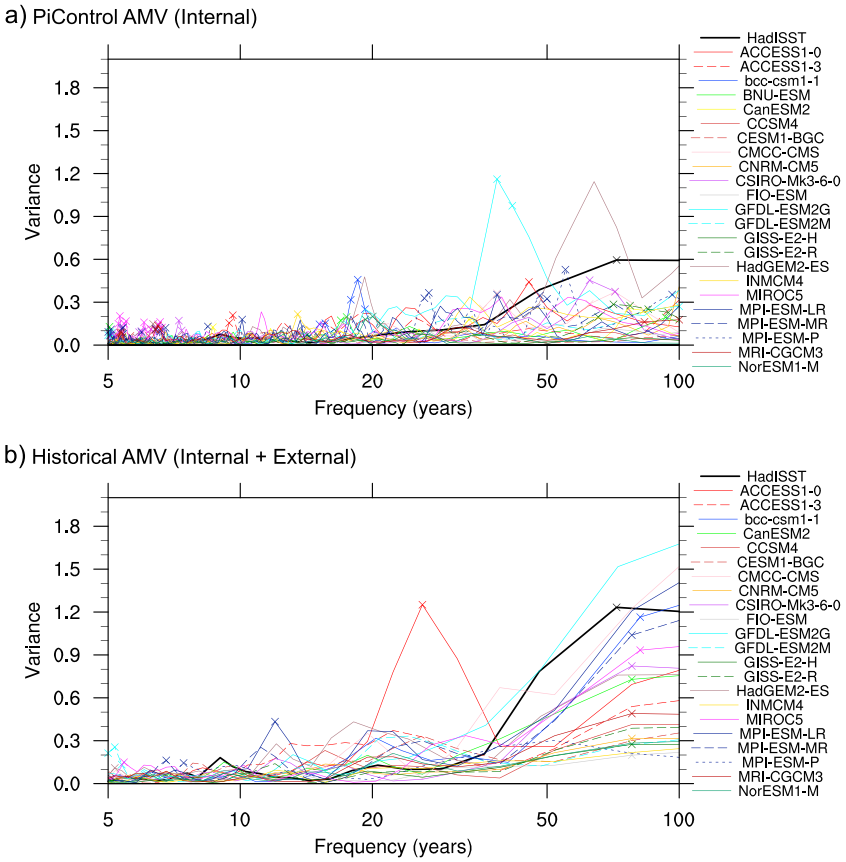

Figure 2. (a) Variance spectra of the observed AMV-gsst index (1870–2013, black line) and of the AMV simulated by CMIP5 models in preindustrial control runs (internal AMV only). (b) Same as Figure 2a but for the observed AMV-detrend index (black line) and the AMV from CMIP5 historical runs (internal + forced component of AMV). Crosses indicate frequencies for which the energy is significantly different from a red noise process (95% confidence level).

to a spatial correlation criterion ($r > 0.25$ between the anomaly and the centroid). The same regime must last for at least 3 days to be selected as a regime occurrence.

3. Results

3.1. AMV Characteristics in CMIP5 Control Runs

The amplitude of multidecadal variability in the AMV time series from the models and observations is evaluated through a Markov spectrum analysis in Figure 2 (the AMV indices are not low-pass filtered for this analysis in order to keep the full spectrum of variability in the time series) and as a ratio of variance of the observed AMV in Table 2 (after filtering the piControl AMV to remove variability that is larger than the length of observations). Figure 2a shows the power spectrum of the AMV index in piControl simulations along with the observed AMV-gsst index to compare the internal AMV from models with our estimate of the unforced AMV in observations. Most of the models exhibit less energy than the observed AMV around the 70 year band for which the peak is significantly above the red-noise confidence interval in observations (as marked by a cross). Two models exhibit large multidecadal variability, GFDL-ESM2G and HadGEM2-ES, with a peak of energy around 45 years and 60 years, respectively (note that the peak of energy at 60 years in HadGEM2-ES is very close to the 95% confidence level). In agreement with Figure 2, these two models are the only ones that exhibit an amount of variance in the 10–144 year window that is comparable to observations (Table 2, ratios close to 1). They also exhibit the largest AMV persistence, as estimated by the *e*-folding time of autocorrelation of the AMV time series (Table 2), which is systematically smaller than in observations (even though the observed persistence is subject to uncertainty, ranging from 7 to 12 years depending on the choice of internal AMV index).

The lack of AMV is not explained by a residual influence of external forcings that could still be present in the observed AMV indices. Indeed, the observed AMV-detrend index, which includes the influence of multidecadal variations in external forcings, also exhibits more energy than similar detrended AMV indices from historical simulations (Figure 2b). This was also noted by *Zhang and Wang* [2013] and supports the idea that most of the CMIP5 models that are analyzed in this study underestimate the amplitude of the AMV. Similar conclusions are obtained when comparing piControl simulations with the AMV-lens and AMV-cmip5 observed indices. As shown on Figure S1 in the supporting information, despite notable differences between the different observed indices, most of the models exhibit less multidecadal variability than any observed-AMV index in the 40–70 year range (see also variance ratios in Table 2). Figure S2 shows the dependence of this result on sample size, by subsetting the piControl-AMV time series in accordance with the length of the observational record (144 years, with no overlap between the different subperiods). Again, most of the simulated AMV time series exhibit less multidecadal variability than in observations, further supporting the statement that our selection of CMIP5 models generally lacks internally generated AMV.

The AMV pattern in each model is shown in Figure 3, along with the observed pattern derived from the HadISST data over 1870–2013 (Figure 3a). At each grid point, the correlation of SST with the AMV index is plotted in shading and the regression of SST onto the AMV index is superimposed in contours (0.3°C interval). As suggested by the grid point correlations, most of the models capture an AMV basin-wide signal and the reverse C shape pattern of SST anomalies, but with varying amplitude among models. Like in observations, maximum SST anomalies are generally found in the North Atlantic subpolar gyre, although these are larger in some models (e.g., GFDL-ESM2G) and smaller in others (e.g., CCSM4, GISS-E2-H, MRI-CGCM3, and NorESM1-M). The amplitude of SST anomalies in the subtropics is considerably smaller than in observations, possibly due to the lack of NAO response to the AMV in the models since subtropical AMV-SST are partially a response to changes in ocean-atmosphere interactions induced by the AMV [*Smirnov and Vimont*, 2012; *Ting et al*., 2014]. Table 2 indicates the agreement between the pattern of AMV in piControl simulations and observations, in terms of spatial correlation *R* and root-mean-square error (RMSE). The simulated AMV are compared to the three indices of internal AMV in observations. While RMSE are quite similar between the three observed indices, spatial correlations are systematically higher with the AMV-gsst index, suggesting that this index efficiently isolates the internal AMV as simulated by the models.

In summary, although the pattern of AMV-SST anomalies is reasonable in CMIP5 models, most of them exhibit less variance at multidecadal time scales and less persistence in AMV than do observations. This is a true limitation for identifying long-term predictability associated with the AMV in these models. However, the variability in amplitude and spatial pattern of AMV among the models presents an opportunity to verify whether the wintertime atmospheric circulation is sensitive to the amplitude of multidecadal SST anomalies in the North Atlantic.

3.2. SST-Heat Flux Relationship in the Mid-North Atlantic

In this section we investigate the relationship between SST and the surface heat flux in the North Atlantic for short ($<$10 yrs) and long ($>$10 yrs) time scales. This is a key issue for assessing the ability of the models to capture the influence of the AMV on the atmosphere. Correlations between the AMV index and the total turbulent heat flux (sensible + latent, positive when directed from the ocean to the atmosphere) are computed for the short-term and long-term components of both the AMV and wintertime heat flux. Correlations are computed with the wintertime (DJFM) heat flux which is our season of interest to detect any impact of the AMV onto the atmospheric circulation. *Gulev et al.* [2013] have examined the relationship between SST and heat flux in the mid-North Atlantic using reconstructed turbulent heat flux over 1880–2007 (see their paper for method). Figure S3 shows the grid point correlation between SST and their reconstructed turbulent heat flux for the short-term and long-term components. In the mid-North Atlantic, negative correlations predominate when short-term components are considered, while positive correlations are found for the long-term components, consistent with *Gulev et al.* [2013]. This suggests that at interannual time scales the atmosphere mainly drives the air-sea heat flux exchanges, while they are driven by the ocean at decadal to multidecadal time scales. Note that the heat flux-SST relationship is quite stationary over the 1880–2007 period, as verified in the supporting information of Gulev *et al.* [2013, Figure S8]. This heat flux-SST relationship is analyzed in the CMIP5 models since it is critical for observing a forcing of the atmosphere by the ocean at long time scales.

As in observations, the models indicate that short-term variations of the ocean are driven by atmospheric stochastic variability (Figure 4a). Except for MRI-CGCM3, all correlations are negative and significant at the 95%

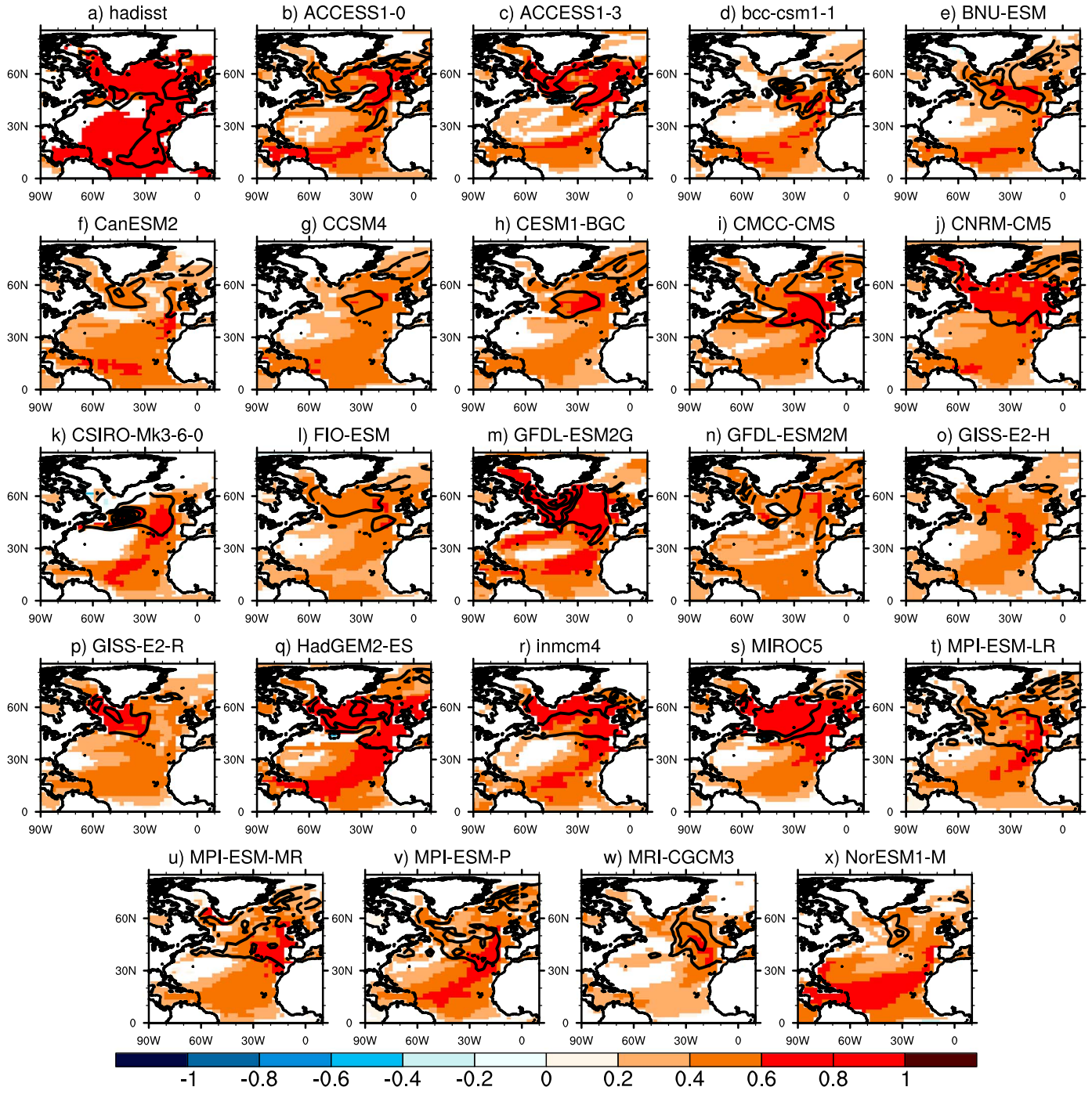

Figure 3. Grid point correlations (shading) and regression (contours, interval 0.3°C) between the annual mean AMV index and the annual SST anomalies for the following: (a) observations (AMV-gsst, 1870–2013 period); (b–x) CMIP5 models. Only correlations that are statistically significant at the 95% confidence level are shown.

confidence level, with a reasonable amplitude compared to observations ($R = -0.44$ in observations, blue dashed line). The heat flux pattern, which is consistent among the models (Figure 4b), resembles the tripole pattern of SST that is forced by the positive phase of the NAO [*Cayan*, 1992]. During the positive NAO, both the westerlies in the storm track region and the easterlies in the subtropics are reinforced, imposing more wind stress to the surface of the ocean. As a consequence, the turbulent heat flux is increased, and SST is colder than normal in the North Atlantic (except for warm anomalies around 30°N that are due to a northward displacement of the jet and reduced surface wind stress in this region).

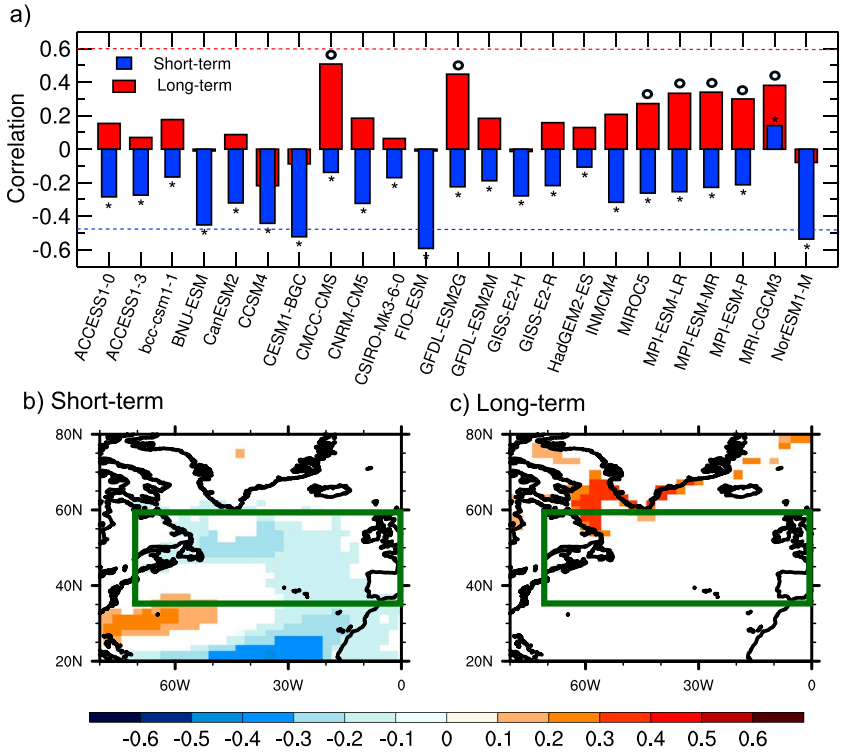

Figure 4. (a) Correlation between the AMV index and the turbulent heat flux (sensible + latent) anomalies in the mid-North Atlantic (35°N/60°N, 70°W/0°E, see box in Figures 4b and 4c) for the short-term (<10 years, blue) and the long-term (>10 years, red) component of the AMV index and heat flux anomalies. Stars and circles indicate correlations that are statistically significant at the 95% confidence level (accounting for autocorrelation in time series) and corresponding observed correlations are shown by dashed lines (1880–2007). (b) Ensemble mean (average of 23 CMIP5 models) of the grid point correlations between the short-term component of AMV index and DJFM turbulent heat flux anomalies. Only grid points where 75% of the models agree on the sign of the correlation are shaded (18 out of 23 models). (c) Same as b but for the long-term component of AMV index and DJFM turbulent heat flux anomalies.

At decadal to multidecadal time scales, most of the models simulate positive correlations between the AMV and heat flux anomalies (Figure 4a), but these are of lower amplitude than in observations ($R = 0.6$ in observations, red dashed line), and they are statistically significant at the 95% confidence level for only seven models. The pattern of long-term correlations differs among the models (Figure S4 shows grid point correlations in individual models) with little agreement on the sign of correlations in the mid-North Atlantic (Figure 4c). This lack of long-term positive SST-heat flux correlations in the mid-North Atlantic limits the ability of the models to simulate a significant influence of the AMV on the long-term fluctuations of the atmosphere. On the other hand, most of the models agree concerning positive correlations in the Labrador Sea (Figure 4c) that are due to the loss of sea ice associated with the positive AMV. Warmer SST in the high-latitude results in significant loss of sea ice concentration in every model (Figure S5). GFDL-ESM2G simulates the largest sea ice loss and heat flux anomalies in the Labrador Sea and subpolar gyre (Figures S4l and S5l), in line with the large amplitude of the AMV in this model (Figures 2a and 3m). The positive AMV has been pointed out in several recent studies as one of the drivers of the recent acceleration of sea ice decline in the Arctic [*Mahajan et al.*, 2011; *Day et al.*, 2012; *Zhang*, 2015; *Yeager et al.*, 2015]. Our results support that natural variability due to AMV alone can account for a significant part of the recent sea ice anomalies of the North Atlantic sector in winter.

3.3. Linkage Between the AMV and the Wintertime NAO

The linkage between the AMV and the wintertime atmospheric circulation is assessed by performing a composite analysis of the DJFM sea level pressure (SLP). For each CMIP5 model, the composite of SLP is constructed by differentiating years of high AMV index (above the higher quartile of the AMV time series) from the years of low AMV index (below the lower quartile of the AMV time series). Results are shown in

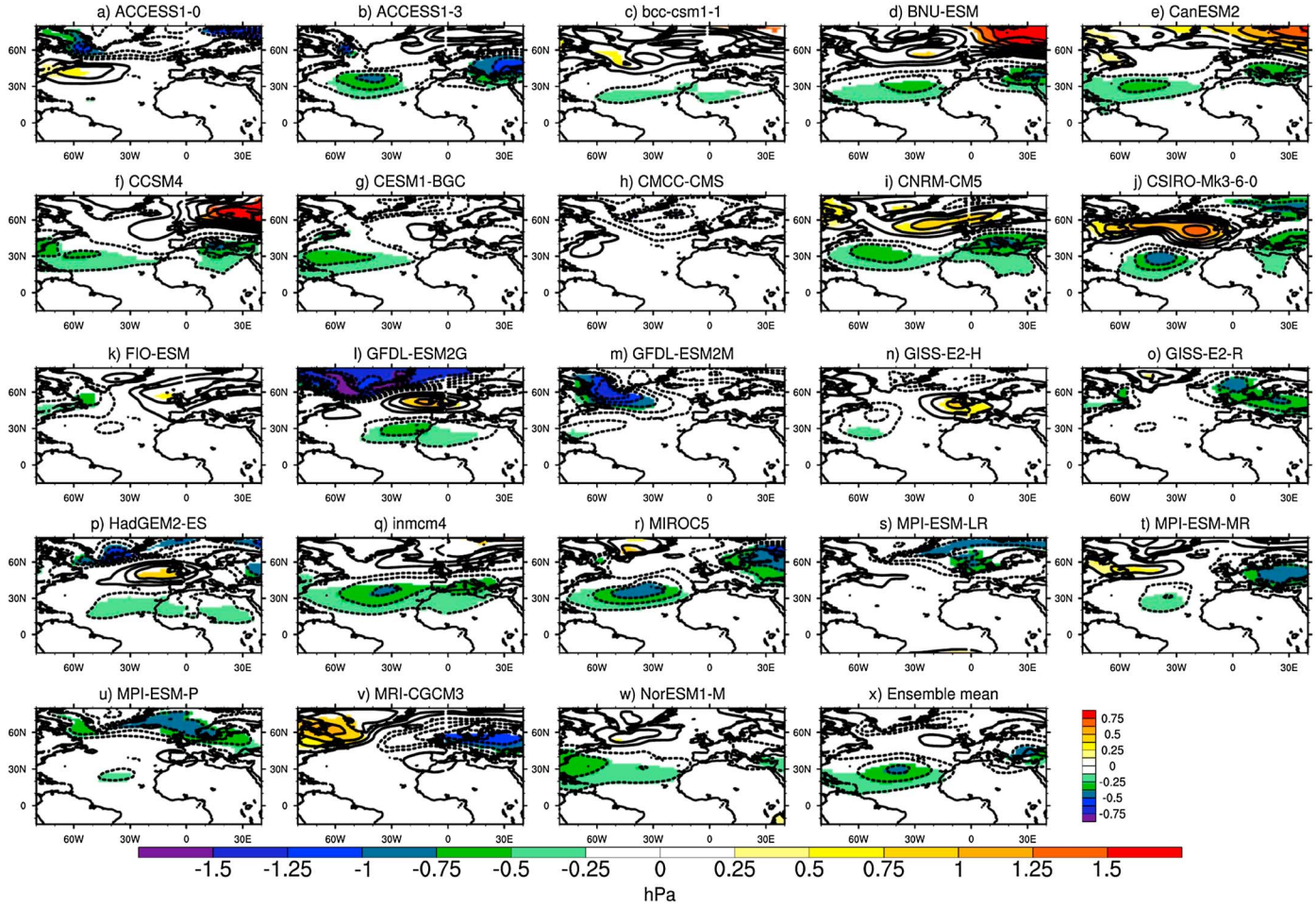

Figure 5. (a–w) Composite of DJFM sea level pressure (hPa) computed as the difference between years with warm and cold AMV (quartile threshold) for each individual CMIP5 model. Anomalies that are significant at the 95% confidence level are shaded. (x) Ensemble mean of the SLP anomalies. Anomalies are shaded when at least 75 % of the models agree on the sign of the SLP anomaly (18 out of 23 models).

Figure 5 for individual models (Figures 5a–5w) and the ensemble mean (Figure 5x). The pattern of SLP differs between the models, except for low SLP anomalies in the subtropical Atlantic that are found in more than 75% of the models (Figure 5x) and are consistent with the effect of SST anomalies in the tropics [*Hoskins and Karoly*, 1981]. In the extratropics, no agreement is found for the sign of SLP anomalies. This does not support the existence of any clear synchronous relationship between the AMV and long-term fluctuations of the NAO. This result is contradictory with results from *Ting et al*. [2014] who have identified a robust negative NAO pattern in CMIP3 models when the AMV is in its warm phase. Reasons for such a discrepancy are unclear and are likely related to both differences in the models (CMIP3 versus CMIP5) and in methodologies.

Lagged composites of SLP are also computed to determine whether any lead-lag relationship between the AMV and the atmospheric circulation exists at multidecadal time scales. Figure 6a shows the low-frequency pattern of SLP that precedes the AMV by 5 years in the models. This time, there is strong agreement between the models and all of them exhibit a robust positive NAO pattern in winters preceding the AMV. The AMV is therefore driven by low-frequency fluctuations of the wintertime NAO in the models, a persistence of positive wintertime NAO being followed by a warm AMV, and vice versa. This is consistent with previous studies that have shown that the persistence of the NAO in a particular phase induces a reinforcement of the AMOC and an associated buildup of the AMV by perturbing the deep convection regions through wind stress and heat flux anomalies (e.g., *Eden and Willebrand*, 2001; *Medhaug et al*., 2012; *Barrier et al*., 2014). On the other hand, when the AMV precedes the atmospheric circulation by 5 years (and at larger lags), no consistent signal is found (Figure 6b), although some models exhibit significant but weak negative correlations. Thus, no consensus exists in the CMIP5 models that

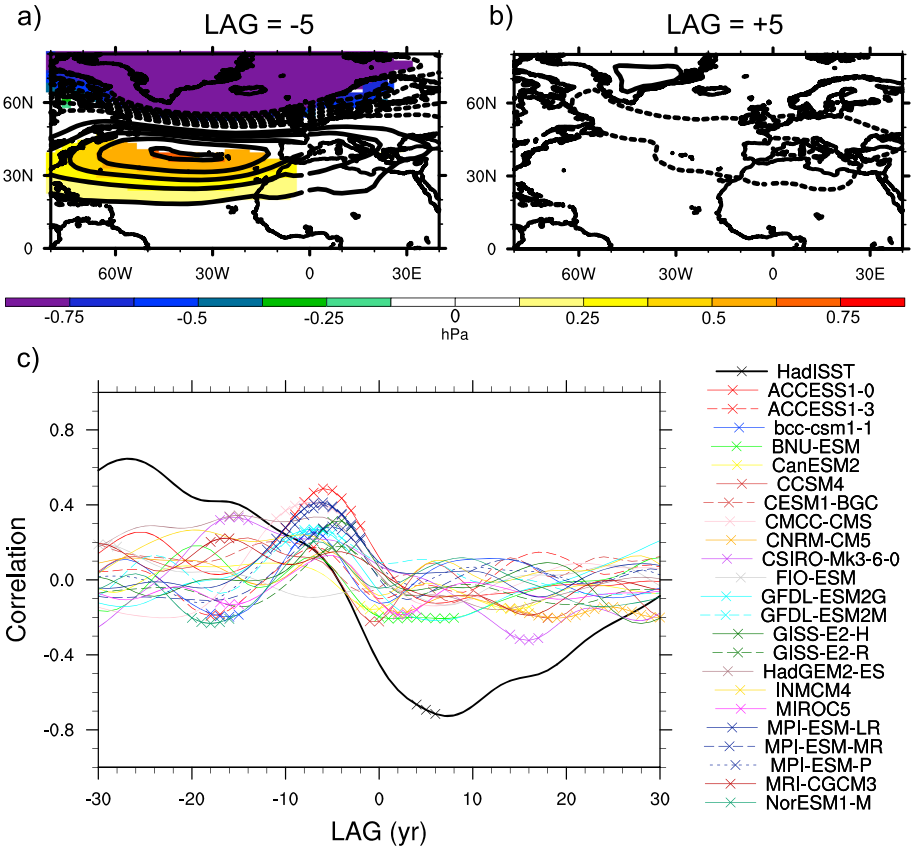

Figure 6. (a) Ensemble mean of DJFM SLP anomalies (hPa) 5 years before the peak of AMV. Anomalies are shaded when at least 75 % of the models agree on the sign of the SLP anomaly (18 out of 23 models). (b) Same as Figure 6a but for DJFM SLP anomalies 5 years after the peak of AMV. (c) Lead-lag correlations between the AMV index and the decadal DJFM NAO index in individual CMIP5 models and in observations (black line, 1901–2010 period). Negative (positive) lags indicate that the NAO precedes (follows) the AMV. Crosses indicate where the correlation is significant at the 95% confidence level based on a phase-scrambled bootstrap test that accounts for autocorrelation in the time series.

would support the presence of a significant feedback from the ocean onto the wintertime atmospheric circulation at long time scales (>10 years). This is also supported by computing lead-lag correlations between the AMV and the winter NAO indices for individual models (Figure 6c). The maximum correlation is found when the NAO leads the AMV of about 5 years, but no large correlation is found when the AMV leads the NAO.

The absence of consistent lagged correlations when the AMV leads the NAO is at odds with results from observations [*Omrani et al.*, 2014; *Peings and Magnusdottir*, 2014]. As shown in Figure 6c (black line), the observed AMV-NAO multidecadal relationship exhibits a "swing" in the lead-lag correlations, from positive values when the NAO leads (the positive NAO is followed by the positive AMV) to negative correlations when the AMV leads (the positive AMV is followed by the negative NAO). Note that the annual AMV index is used here, explaining small differences with the lead-lag correlations of *Peings and Magnusdottir* [2014] that used a DJFM AMV index. These lead-lag correlations suggest that a two-way interaction exist between the AMV and the NAO at multidecadal time scales. However, observations are short (only two cycles of the AMV) and we cannot rule out the possibility that this apparent relationship represents a statistical artifact without any physical meaning (although numerical experiments suggest the opposite, e.g., *Peings and Magnusdottir* [2015]).

Due to their length, the CMIP5 simulations can give us a hint about this question. If lead-lag correlations similar to those found in observations can be detected during subperiods of the piControl simulations, even though such correlations are absent when computed from the entire period, that would suggest that the observed AMV-NAO signal is non-stationary or can happen by chance and thus that it is not a robust feature of the North Atlantic. To the contrary, the absence of a similar lead-lag relationship in any of the piControl

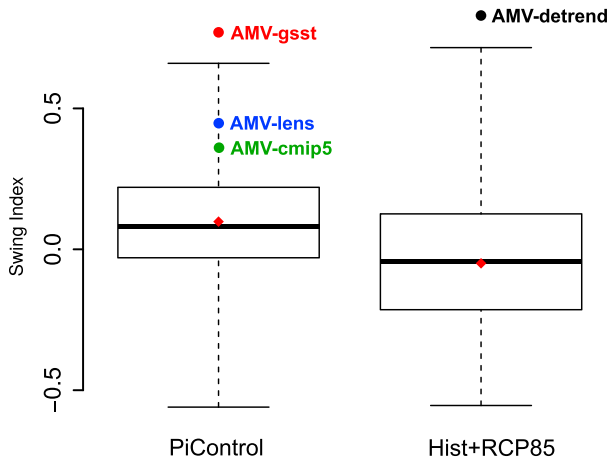

Figure 7. Distribution of the swing index (swing in AMV-NAO correlation from negative to positive lags; see text and Figure 6c) in 126 subperiods of the (left) piControl simulations and in 53 subperiods of the (right) historical/RCP8.5 simulations. Subperiods are 110 year long to match the length of observations and are independent (no overlap). Values of the swing index (1901–2010) for the four observed AMV indices are shown as a reference. Box plots indicate the maximum, upper quartile, median, lower quartile, and minimum of the distribution (horizontal bars). The mean of the distribution is shown by a red diamond.

subperiods would support the idea that the observed AMV-NAO relationship is not a simple coincidence and that the models are missing certain processes to capture this low-frequency teleconnection.

For each model, the AMV and NAO time series are split into several subperiods of 110 year length, as in observations (we select the 1901–2010 period for observations, to be consistent with *Peings and Magnusdottir* [2014]). For instance, four subperiods are extracted from the 500 year long ACCESS1-0 piControl simulation. Similar lead-lag correlations to Figure 6c are then recomputed for each individual subperiod of each model. In order to give an objective criterion for the similarity between the shape of lead-lag correlations in observations and in the model subperiods (presence or absence of a swing at lag 0), an index (the "swing index") is computed that represents the difference between the averaged correlations at negative lags (−30 to 0), and the averaged correlations at positive lags (0 to +30). For observations, the value of the swing index is 0.77 in Figure 6c (AMV-gsst). It is 0.83 for AMV-detrend, 0.33 for AMV-cmip5, and 0.44 for AMV-lens. The distribution of this index as simulated by the models (13,860 years of piControl simulations, i.e., 126 independent subperiods) is plotted through a box plot-whisker representation and compared to the observed values in Figure 7. The swing index has also been computed for historical/RCP8.5 simulations (from the detrended AMV index) to verify that the results do not depend on the presence of external forcings (5830 years, 53 independent subperiods). All simulated swing index values that are used to plot the distributions are independent since there is no overlap between the different subperiods.

As shown in Figure 7, no subperiods of the piControl (compared to AMV-gsst) and historical/RCP8.5 (compared to AMV-detrend) exhibit a swing index value that is as large as in observations. Note that this result is also found when subperiods are selected using a 10 year moving window, retaining a considerably larger number of subperiods (1244 for piControl, 416 for historical/RCP8.5) that are not independent because of the overlap. In this case, two subperiods exhibit a larger correlation in piControl simulations (both from HadGEM2-ES), one in historical/RCP8.5 (from bcc-csm1-1), such that the observed values of the swing index from AMV-gsst and AMV-detrend still constitute an outlier for the distribution of the swing index in the simulations (not shown). The swing index, although still in the upper range of the model distribution, is smaller when computed from AMV-cmip5 and AMV-lens, highlighting the large uncertainty in the observed AMV. Although this uncertainty in the observed AMV have to be kept in mind, the present analysis suggests that the CMIP5 models are missing, or at best underestimating, the two-way interaction between the AMV and the NAO on multidecadal time scales, regardless of the presence of external forcings.

The absence of a significant feedback of the AMV onto the NAO in the models is consistent with their underestimate of the AMV (section 3.1) and with the absence or underestimate of ocean-atmosphere heat flux forcing in the mid-North Atlantic (section 3.2). Even when considering the seven models that simulate a statistically significant positive correlation between AMV and heat flux in the mid-North

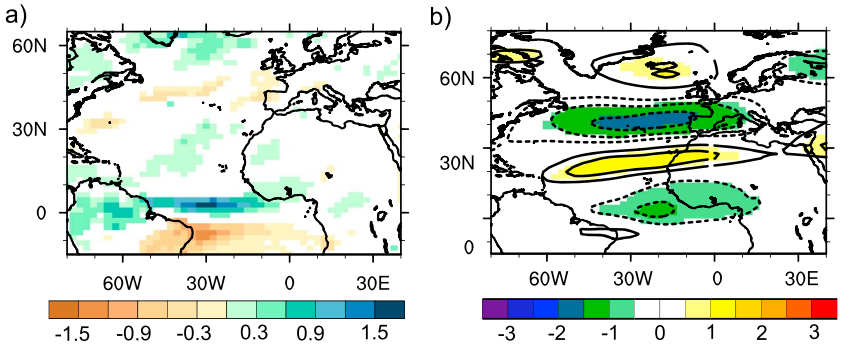

Figure 8. (a) Composite of the DJFM precipitation (mm/d) computed as the difference between years with warm and cold AMV (quartile threshold) for HadGEM2-ES. Only anomalies that are statistically significant at the 95% confidence level are shown. (b) Same as Figure 8a but for the DJFM 200 hPa zonal wind (m/s). Anomalies that are statistically significant at the 95% confidence level are shaded.

Atlantic (CMCC-CMS, GFDL-ESM2G, MIROC5, MPI-ESM-LR, MPI-ESM-MR, MPI-ESM-P, and MRI-CGCM3; Figure 4a), the patterns of SLP anomalies (Figure 5), and the lagged AMV-NAO correlations (Figure 6c) are inconsistent.

In addition to midlatitude heat flux forcing, another important process for simulating a significant modulation of the wintertime NAO by the AMV is a perturbation of the Intertropical Convergence Zone (ITCZ) in the equatorial Atlantic. A change in ITCZ has been identified using different AGCM perturbation experiments as a response to the AMV forcing [*Sutton and Hodson*, 2007; *Ting et al*., 2011, *Peings and Magnusdottir*, 2015, *Davini et al*. 2015]. Warm tropical AMV-SST anomalies perturb the meridional gradient of SST and shift the Atlantic ITCZ north of the equator. Displacement of the ITCZ, and thus the local Hadley cell, induces heating anomalies and upper level divergence that generates a Rossby wave train in the free troposphere. The propagation of Rossby waves from the tropics into the extratropics has been found to be the main mechanism that explains the NAO response to tropical Atlantic SST anomalies [*Okumura et al*., 2001; *Terray and Cassou*, 2002; *Drevillon et al*., 2003; *Sutton and Hodson*, 2007; *Peings and Magnusdottir*, 2015; *Davini et al*. 2015]. The pattern of wintertime precipitation associated with the AMV in the models is shown on Figure S6. Some models exhibit a northward shift of the ITCZ in the equatorial Atlantic, but the amplitude of the signal is generally small. The only model that shows a large signal is HadGEM2-ES (Figure 8a). A dipole of precipitation is present in the equatorial Atlantic (northward shift of the ITCZ) that resembles the precipitation response identified in AMV perturbation experiments in atmospheric GCMs [e.g., *Peings and Magnusdottir*, 2015; *Davini et al*. 2015]. HadGEM2-ES is one of the models that has the largest AMV signature in the subtropics (Figure 3q) and hence the largest potential for simulating a significant perturbation of the ITCZ. As expected from the ITCZ anomaly, a Rossby wave is visible in the North Atlantic, with an alternation between negative and positive 200 hPa zonal wind anomalies from the tropics into the extratropics (Figure 8b). This signal, which is not found in other models (not shown), is consistent with the small but significant NAO pattern that is associated with the AMV in this model. The NAO signal is mostly present in late winter (February–March), 10 years after the peak of the AMV (see the lagged composites of the FM SLP in HadGEM2-ES in Figure S7). This is consistent with observational results from *Peings and Magnusdottir* [2014], who found a larger response of the NAO to the AMV in late winter. Although a small signal, the results from HadGEM2-ES support findings from perturbation experiments that the NAO is modulated when the AMV is associated with a substantial perturbation of the ITCZ location in winter. Note that HadGEM2-ES has been suggested as a model that overestimates the impact of aerosol indirect effects [*Zhang et al*., 2013], such that the role of subtropical SST might be exaggerated in the piControl simulation of this model due to an unrealistic influence of natural aerosols.

Finally, it is important to note that the subtropical component of AMV-SST anomalies in observations is possibly a response to the NAO pattern that is associated with the AMV [*Penland and Hartten*, 2014]. The absence of any large subtropical AMV-SST anomalies and associated perturbation of the ITCZ in the CMIP5 models might thus be due to the absence of NAO response to the AMV.

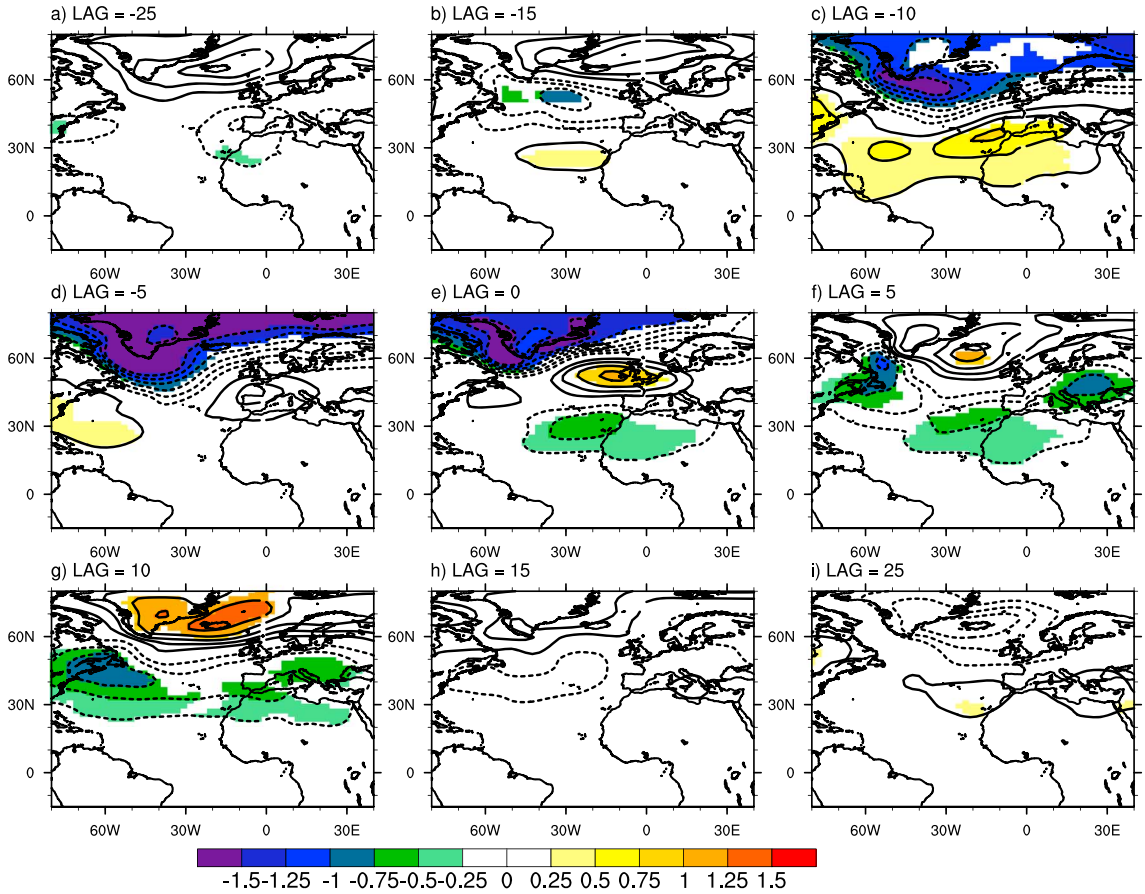

Figure 9. Lagged composites of DJFM sea level pressure (hPa) computed as the difference between years with warm and cold AMV (quartile threshold) for GFDL-ESM2G. A negative (positive) lag indicates that the AMV follows (precedes) the SLP anomalies. Anomalies that are statistically significant at the 95% confidence level are shaded.

3.4. Focus on the GFDL-ESM2G Model

3.4.1. Interactions Between AMV, AMOC, NAO, and Sea Ice

Another model of interest is GFDL-ESM2G, since this model is the only one that meets all the following criteria: a large amplitude of the AMV (Figure 2), a statistically significant and large positive correlation between heat flux and SST in the mid-North Atlantic (Figure 4a), and a negative NAO pattern following the peak of the positive AMV, as shown subsequently. Figure 9 shows the evolution of the SLP anomalies with the buildup of the AMV in this model (lags from −25 to +25 years before and after the peak of AMV). Similar to the other models, the AMV in GFDL-ESM2G is preceded by a positive NAO pattern that emerges around lag −15 years (Figure 9b). SLP anomalies then progressively turn into a negative NAO pattern that reaches maximum amplitude at lag +10 years (Figure 9g). The SLP anomalies are associated with negative sea ice anomalies that emerge in the Labrador Sea at lag −15 and extend to the Greenland Sea (Figure S8) as the AMV builds in the North Atlantic (Figure S9). This sequence of events suggests that the following mechanism is at work in GFDL-ESM2G, in agreement with previous analyses of air-sea interactions in the North Atlantic that used coupled ocean-atmosphere control runs [*Gastineau et al.*, 2013; *Ruprich-Robert and Cassou*, 2014]. Persistence of the positive phase of the NAO in winter induces wind stress and heat flux anomalies in the subpolar gyre. The advection of dense salty water in the gyre reinforces the AMOC by increasing the deep convection in the Labrador and Greenland seas. In response to warmer SST, sea ice decreases in these two regions (Figure S8). The AMV builds with the increase of the AMOC (Figure S9), and the positive NAO pattern that triggered the process is progressively replaced by a negative NAO, the signature of the oceanic feedback onto the atmosphere (Figures 9e–9g). The timing of these different events is illustrated in Figure 10, which shows lead-lag correlations between the wintertime NAO, the AMOC, the AMV, and sea ice anomalies in the Labrador Sea area in winter. A persistent

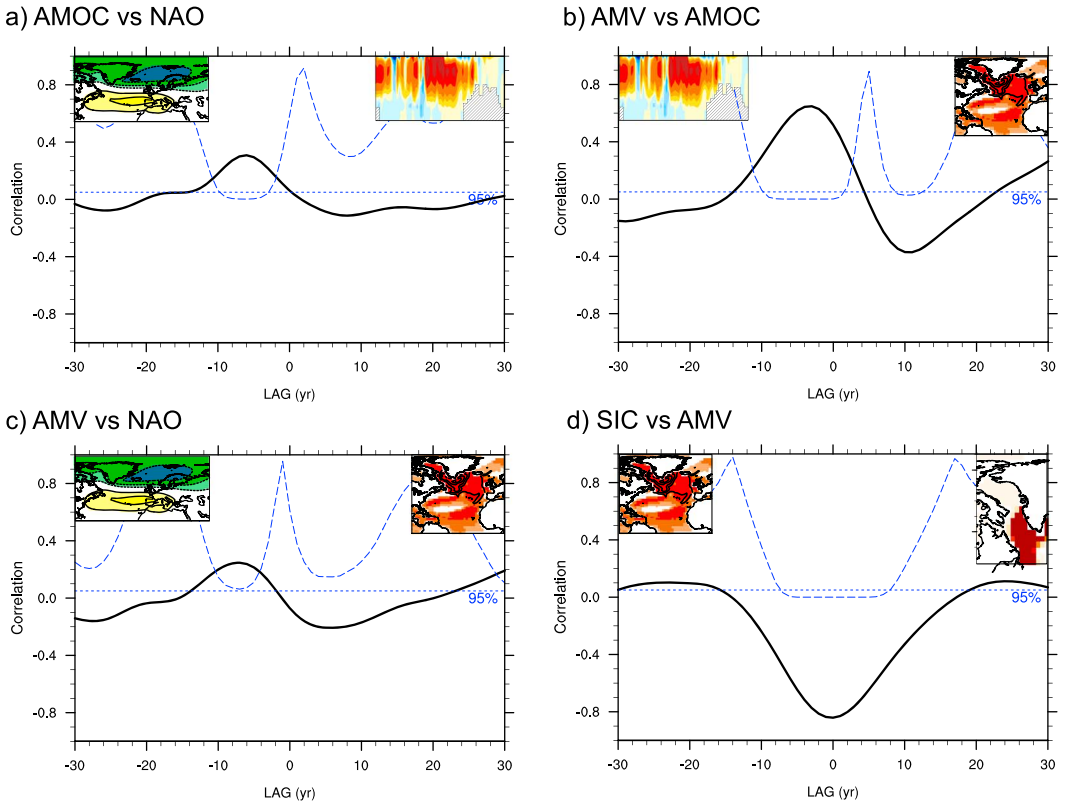

Figure 10. Lead-lag correlations in GFDL-ESM2G between the following: (a) the AMOC and the decadal DJFM NAO index (black line). Negative (positive) lags indicate that the NAO precedes (follows) the AMOC. The statistical significance of the correlations is depicted by the *p* value (blue dashed curve), computed using a phase-scrambled bootstrap method that accounts for autocorrelations in the time series. The 95% confidence level is indicated by the dashed blue line. (b) Same as Figure 10a but for lead-lag correlations between the AMV and the AMOC. (c) Same as Figure 10a but for lead-lag correlations between the NAO and the AMV. (d) Same as Figure 10a but for lead-lag correlations between the AMV and sea ice concentration anomalies in the Labrador sea (see region in the upper right corner of the plot).

positive winter NAO precedes the peak of AMOC by about 5–10 years (Figure 10a). The positive AMV builds as the AMOC reinforces and peaks about 5 years after the maximum in AMOC (Figure 10b). Figure 10c shows that the synchronous AMV-NAO correlation is negative. The synchronous relationship mainly reflects the forcing of the atmosphere onto the ocean since negative NAO-driven tripolar SST anomalies project onto the AMO [*Hurrell et al.*, 2003]. However, like in observations, the maximum negative correlation is seen 5–10 years after the peak of the AMV [*Peings and Magnusdottir*, 2014; *Gastineau and Frankignoul*, 2015], suggesting that the ocean, in turn, exerts a feedback onto the atmosphere. Although not significant at the 95% confidence level as will be discussed below, this correlation likely reflects the forcing imposed to the NAO by the AMV. Warmer SST into the subpolar latitudes also leads a significant sea ice loss in the Labrador Sea that coincides with the peak of the AMV (Figure 10d).

3.4.2. AMV and Synoptic Variability of the Atmosphere

Given that large tropical SST and precipitation anomalies are absent in GFDL-ESM2G, the apparent NAO response to the AMV must essentially arise from a forcing mechanism in the extratropics. GFDL-ESM2G simulates particularly large SST and sea ice anomalies in the North Atlantic subpolar gyre in association with the AMV (Figure 3m and S5l). It is well-known that SST anomalies in the North Atlantic subpolar gyre and in the Gulf stream region have the potential to induce significant perturbations to the North Atlantic storm tracks through changes in baroclinicity in the troposphere [*Peng et al.*, 2005; *Sutton and Hodson*, 2007; *Minobe et al.*, 2008; *Nakamura et al.*, 2008; *Peings and Magnusdottir*, 2015]. In order to investigate whether such a mechanism is at work in GFDL-ESM2G, Figure 11 shows lagged composites of the storm track activity over the Atlantic. The transient eddy activity is computed as the standard deviation of the daily Z500. Consistent with the existence of a forcing mechanism involving eddy-mean flow interactions, a shift then a decrease in transient eddy activity is

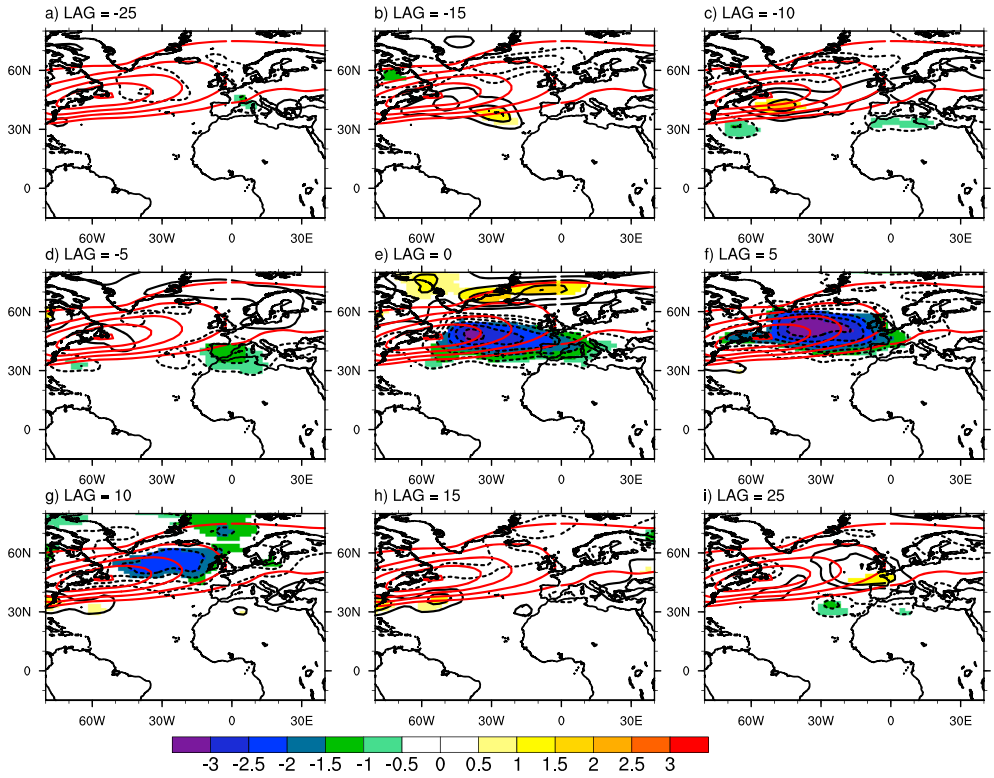

Figure 11. Same as Figure 9 but for the transient eddy activity (monthly standard deviation of the 2–6 days filtered Z500). Climatology is given in red contours (contour interval 6 m from 30 to 60 m).

visible in the mid-North Atlantic from lag 0 to +10 years. Maximum negative anomalies are located downstream of the core of storm track activity (see climatology in red contours), at the exit of the polar front jet stream. A decrease in transient eddy activity feed backs on the large-scale circulation and promotes the negative NAO pattern in winter [*Hoskins et al*., 1983]. This change in storm track activity has been identified in observational analyses and perturbation experiments as a major feature of the atmospheric response to the AMV [*Peings and Magnusdottir*, 2014, *Davini et al*. 2015, *Gastineau and Frankignoul*, 2015].

In order to further characterize the atmospheric response to the AMV, we compute the change in frequency of the main weather regimes that describe a large portion of the wintertime synoptic variability over the North-Atlantic (see section 2.3 for methods). The NAO is not the only wintertime atmospheric mode of variability that may be impacted by the AMV variability over the North-Atlantic sector. For example, the frequency of atmospheric blocking has been shown to be modulated by the AMV [*Häkkinen et al*., 2011; *Peings and Magnusdottir*, 2014, *Davini et al*. 2015]. Four weather regimes are commonly identified by the weather regime methodology, i.e., the Atlantic Ridge, the Blocking, the negative NAO (also referred as to Atlantic low), and the positive NAO [*Cassou*, 2008]. Each of these weather regimes has a different signature in terms of temperature and precipitation anomalies over Europe and the eastern North America. For instance, the negative NAO brings colder conditions over northwestern Europe and the eastern U.S. in winter. The blocking regime is often associated with frigid temperature in central/western Europe due to the advection of cold air from Siberia. The response of these four weather regimes to the AMV has been investigated in *Peings and Magnusdottir* [2014] in both the 20CR reanalysis and perturbation experiments using the Community Atmospheric Model version 5 (CAM5) AGCM. A significant shift in the frequency of the NAO with the AMV polarity was found in 20CR and in CAM5 experiments. A warm AMV increases the occurrence of NAO− days at the expense of NAO+ days, especially in late winter. We found this to be associated with an increase in cold extreme days in northwestern Europe and eastern U.S., suggesting that the current positive phase of the AMV might be partly responsible for a resurgence of cold extreme events in winter in these regions.

Changes in the frequency of weather regimes with the AMV are investigated in GFDL-ESM2G by comparing years of warm and cold AMV (Figure 12). The four predominant wintertime weather regimes in the model

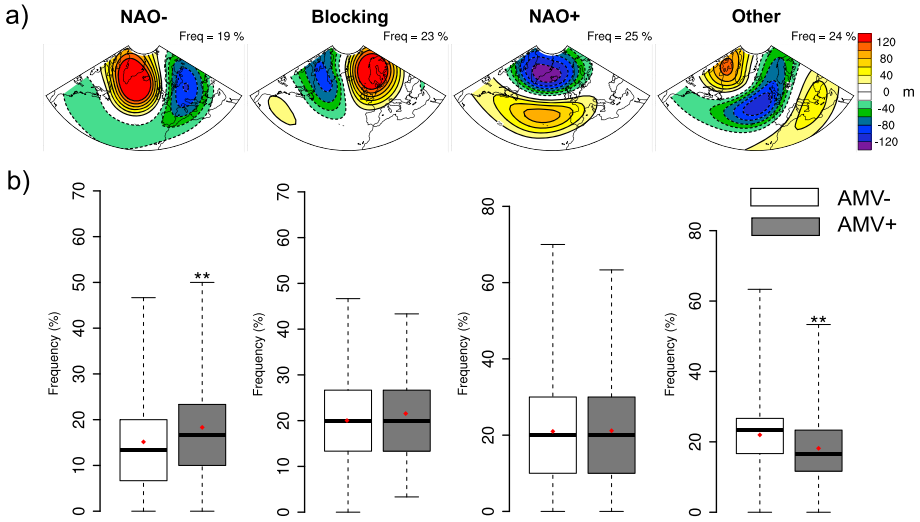

Figure 12. (a) DJFM North Atlantic weather regimes in GFDL-ESM2G, computed from the daily Z500 anomalies (in m). Frequencies of occurrence in percent of wintertime days are indicated. (b) Distribution of the winter regime frequencies in GFDL-ESM2G for years with a cold AMV (white box plots) and a warm AMV (grey box plots). Box plots indicate the maximum, upper quartile, median, lower quartile, and minimum of the distribution (horizontal bars). The mean of the distribution is shown by red diamonds. Asterisks indicate that the difference of the mean between warm and cold AMV years is statistically significant to the 95% confidence level.

are shown in Figure 12a. They account for 91% of the winter days; NAO+ being the most frequent weather regime in the climatology (as in observations). The two NAO regimes are detected, as well as the blocking regime. However, the Atlantic Ridge regime is absent from this analysis and replaced by a regime that we refer to as "OTHER." OTHER consists of a tripole of Z500 anomalies over the region resembling a combination of the NAO− and NAO+ regimes. Except for OTHER, the three usual weather regimes exhibit spatial patterns and climatological frequencies that are in rather good agreement with observations [*Cassou*, 2008]. Figure 12b shows the change in the distribution of the winter frequencies for each regime, for years with a warm AMV (grey box plot) and years with a cold AMV (white box plot). In line with *Peings and Magnusdottir* [2014], warm AMV periods are associated with a larger occurrence of NAO− that is statistically significant at the 95% confidence level. Nevertheless, unlike in 20CR and CAM5 experiments, this is compensated in GFDL-ESM2G not by a decrease in NAO+ but rather by a decrease in OTHER. This nonlinearity between changes in NAO− and NAO+ may explain why we do not find a larger correlation between the monthly NAO index and the AMV at positive lags in Figure 10c. Unlike in *Peings and Magnusdottir* [2014] and *Häkkinen et al*. [2011], the blocking regime is not impacted by the AMV in GFDL-ESM2G. When a lag is considered for computing the distribution of weather regimes frequencies for each AMV phase, our findings are consistent with results using monthly data. In fact, the frequency of NAO+ is increased 5 to 10 years before the peak of the AMV as in Figure 10c (not shown). Moreover, the increase in NAO− with the warm AMV persists and remains statistically significant 5 to 10 years after the peak of AMV. These results support the presence of a significant feedback of the AMV onto the wintertime atmospheric circulation at multidecadal time scales, which materializes through a shift in the intraseasonal distribution of typical weather patterns of the North Atlantic region. Nonetheless, the response of cold extremes over Europe and eastern North America is small in GFDL-ESM2G (not shown), indicating that the dynamical response in this model is not pronounced enough to significantly impact the surface temperature.

4. Conclusions

This study evaluates the internally generated AMV in preindustrial control simulations from 23 CMIP5 models and explores whether the AMV exerts a feedback on the atmospheric circulation in winter. Two models, GFDL-ESM2G and HadGEM2-ES, simulate a large AMV while other models show small multidecadal variability in the 40–70 year peak of AMV in observations. Although large uncertainties exist in observations, this result is found for three different observed AMV indices (these indices differ in the methodology that is used to isolate the internal component of the AMV from multidecadal variability forced by external drivers, such as volcanic

eruptions and anthropogenic emissions). Comparisons between the observed linearly detrended AMV index and similar detrended AMV from historical/RCP85 simulations lead to consistent conclusions, further supporting that the apparent underestimate of the AMV in the models does not arise from residual forced variability in the observed AMV indices. On the other hand, all the models capture a realistic basin-wide pattern of AMV-SST anomalies, although the amplitude of SST anomalies is generally smaller than in observations, especially in the subtropical Atlantic.

In most of the CMIP5 models and in agreement with previous studies [e.g., *Medhaug and Furevik*, 2011], the NAO is a driver of the AMV, a multiannual persistence of the positive NAO in winter being followed by the warm AMV some years later. However, the potential feedback of the ocean that is identified in observations around 5 years after the peak of the AMV is not identified in the models. It is likely related to the underestimation of AMV amplitude in the models. Most of the models capture positive correlations between mid-North Atlantic SST and turbulent heat flux at long time scales (greater than 10 years), but the correlations are smaller than in observations and attain maximum amplitude in the Labrador and Greenland seas rather than in the mid-North Atlantic. Although the observed long-term correlation between SST and heat flux in the mid-North Atlantic is subject to uncertainty [*Gulev et al*., 2013], it is plausible that the state of the art ocean-atmosphere coupled models misrepresent some critical processes to capture this driving role of the ocean on long-term heat flux variability. The absence of lead-lag AMV-NAO correlations similar to observations in subperiods of both the piControl and historical/RCP8.5 simulations also supports the suggestion that the models lack natural variability at multidecadal time scales in the North Atlantic. However, uncertainties in the proportion of internal versus forced AMV in observations prevent us from making firm conclusions. Further work, using longer data sets and/or novel methodologies, will be necessary to confirm or refute the robustness of the AMV-NAO relationship in observations. Meanwhile, these findings raise some interesting prospects for decadal forecasting as they suggest that the current generation of coupled ocean-atmosphere models may underestimate the unforced AMV and the associated impacts on the wintertime atmospheric circulation.

Note that the two models that exhibit a large AMV also show a negative-NAO pattern in winter during and after the peak of the warm AMV. In the case of HadGEM2-ES, the negative NAO is found in late winter only and seems to be mainly driven by the tropical component of the AMV. A shift in the ITCZ, represented by a dipole of precipitation anomalies at the equator, is associated with the AMV in this model. The associated deep convection and upper level divergence anomalies induce the propagation of a Rossby wave train into the extratropics. This teleconnection is consistent with previous studies that have investigated the influence of tropical Atlantic SST anomalies on the atmosphere [e.g., *Sutton and Hodson*, 2007].

GFDL-ESM2G also exhibits a feedback of the ocean onto the atmosphere that resembles observations [*Peings and Magnusdottir*, 2014]. The winter NAO partly drives the AMOC and the associated AMV and sea ice anomalies, following which the ocean seems to exert a negative feedback onto the NAO. Indeed, frequencies of occurrence of the predominant weather regimes of the Euro-Atlantic sector shift depending on the AMV polarity. The NAO- regime is promoted when the AMV is warm, and vice versa. Unlike HadGEM2-ES, no significant perturbation of the ITCZ is identified, nor is a tropical-extratropical Rossby wave train detected, such that the NAO response is likely driven by midlatitude SST and sea ice anomalies. Similar to our AGCM perturbation experiments [*Peings and Magnusdottir*, 2014; *Peings and Magnusdottir*, 2015], storm track activity decreases over the mid-North Atlantic, suggesting that the negative NAO pattern is driven by a change in baroclinicity and eddy-mean flow interactions in the vicinity of the jet stream. However, GFDL-ESM2G tends to overestimate the AMV-SST anomalies in the subpolar gyre and may therefore exaggerate the effect of AMV on the atmospheric circulation.

Another interesting finding is that in the models, the largest heat flux signal associated with the AMV is due to sea ice extent variability in the subpolar North Atlantic. This influence of AMV on sea ice variability is consistent with recent studies that suggest that the AMV (as well as other internal modes of variability of the ocean-atmosphere system) is responsible for a significant portion of the recent loss of sea ice in the Arctic [*Mahajan et al*., 2011; *Day et al*., 2012; *Zhang*, 2015]. Our analysis shows that without any external forcing, sea ice exhibits substantial multidecadal variability in winter in the North Atlantic sector of the Arctic ocean due to the AMV. The impact of the AMV on Arctic sea ice variability therefore needs to be considered when trying to attribute the recent anomalies in the atmospheric circulation to anomalies in Arctic sea ice extent. Indeed, the recent resurgence of cold extremes in winter in the North Atlantic region [*Cohen et al*., 2014], which

has been related to a wavier jet stream [*Francis and Vavrus*, 2015; *Overland et al*., 2015], might be partly driven by SST and sea ice anomalies associated with the AMV [*Peings and Magnusdottir*, 2014; *Sato et al*., 2014; *Mori et al*., 2014] rather than by the anthropogenic forcing. Furthermore, natural variability of the atmosphere is large, especially in midlatitudes, such that attributing short trends of the atmospheric circulation to any boundary forcing is challenging [*Wallace et al*., 2014].

Although the present multimodel analysis show model-dependent results, this study points out different perspectives for future work on the multidecadal predictability associated with the AMV. A better understanding of the nature of the AMV and of the importance of the unforced versus externally forced components is critical for determining any predictability associated with the AMV. This study suggests that the internal component of the AMV is too small in the CMIP5 models, even though considerable uncertainties remain in estimating the internal component of the observed AMV. We have considered the AMV as a basin-wide pattern, but distinguishing the midlatitude/subpolar AMV from the subtropical AMV will help to further understand and evaluate the models, since different processes are responsible for multidecadal SST variability in these regions [*Terray*, 2012].

This study has highlighted two previously identified mechanisms to explain the impact of the AMV on the NAO, i. e., the tropical-extratropical Rossby wave train and the transient eddy activity anomalies induced by heat flux perturbations in the mid-North Atlantic. A third mechanism has recently been shown to be important for simulating a significant response of the NAO to the AMV forcing, the perturbation of the stratospheric polar vortex through propagation of planetary waves into the stratosphere [*Omrani et al*., 2014, 2015]. No consistent stratospheric signal is associated with the AMV in the models (verified by using the 10 hPa zonal wind, not shown). Nevertheless, only two high-top models have been analyzed in this study (CMCC-CMS and MPI-ESM-MR), two models that exhibit a small AMV. Further work using high-top models will therefore be necessary to clarify the importance of the stratospheric mechanism in the AMV-NAO teleconnection.

Acknowledgments
This work was supported by NSF grant AGS-1407360. We would like to thank the different modeling groups that have contributed to the CMIP5 project and the World Data Center Climate at DKRZ for providing the CMIP5 data on the CERA portal (http://cera-www.dkrz.de/WDCC/ui/). We also thank two anonymous reviewers for their constructive comments that helped to improve the manuscript, as well as Julien Cattiaux and Gan Zhang for fruitful discussions during the writing of this paper.

References

Barrier, N., C. Cassou, J. Deshayes, and A.-M. Treguier (2014), Response of North Atlantic Ocean circulation to atmospheric weather regimes, *J. Phys. Oceanogr.*, *44*, 179–201.

Bersch M. (2002) North Atlantic Oscillation–induced changes of the upper layer circulation in the northern North Atlantic Ocean. *J. Geophys. Res.*, *107*(C10), 3156, doi:10.1029/2001JC000901.

Bjerknes, J. (1964), Atlantic air-sea interaction, *Adv. Geophys.*, *10*, 1–82.

Booth, B. B. B., N. J. Dunstone, P. R. Halloran, T. Andrews, and N. Bellouin (2012), Aerosols implicated as a prime driver of twentieth-century North Atlantic climate variability, *Nature*, *484*, 228–232, doi:10.1038/Nature11138.

Cassou, C. (2008), Intraseasonal interaction between the Madden-Julian Oscillation and the North Atlantic Oscillation, *Nature*, *455*(7212), 523–527, doi:10.1038/nature07286.

Cayan, D. R. (1992), Latent and sensible heat flux anomalies over the northern oceans: Driving the sea surface temperature, *J. Phys. Oceanogr.*, *22*, 859–881.

Chen, H., and E. K. Schneider (2014), Comparison of the SST forced responses between coupled and uncoupled climate simulations, *J. Clim.*, *27*, 740–756, doi:10.1175/jcli-d-13-00092.1.

Chen, H., E. K. Schneider, B. P. Kirtman, and I. Colfescu (2013), Evaluation of weather noise and its role in climate model simulations, *J. Clim.*, *26*, 3766–3784, doi:10.1175/JCLI-D-12-00292.1.

Cohen, J., et al. (2014), Recent Arctic amplification and extreme mid-latitude weather, *Nat. Geosci.*, *7*, 627–637.

Compo, G. P., et al. (2011), The twentieth century reanalysis project, *Q. J. Geol. Meteorol. Soc.*, *137*, 1–28.

Cunningham, S. A., et al. (2007), Temporal variability of the Atlantic meridional overturning circulation at 26.5°N, *Science*, *17*, 935–938.

Davini, P., J. von Hardenberg, and S. Corti (2015), Tropical origin for the impacts of the Atlantic Multidecadal Variability on the Euro-Atlantic climate, *Environ. Res. Lett.*, *10*, 094010, doi:10.1088/1748-9326/10/9/094010.

Davison, A. C., and D. V. Hinkley (1997), *Bootstrap Methods and Their Application*, 582 pp., Cambridge Univ. Press, New York.

Day, J. J., J. C. Hargreaves, J. D. Annan, and A. Abe-Ouchi (2012), Sources of multi-decadal variability in Arctic sea ice extent, *Env. Res. Lett.*, *7*, 034011, doi:10.1088/1748-9326/7/3/034011.

DelSole, T., M. K. Tippett, and J. Shukla (2011), A significant component of unforced multidecadal variability in the recent acceleration of global warming, *J. Clim.*, *24*, 909–926, doi:10.1175/2010JCLI3659.1.

Delworth, T. L., and E. M. Mann (2000), Observed and simulated multidecadal variability in the Northern Hemisphere, *Clim. Dyn.*, *16*, 661–676.

Delworth, T., S. Manabe, and R. J. Stouffer (1993), Interdecadal variations of the thermohaline circulation in a coupled ocean–atmosphere model, *J. Clim.*, *6*, 1993–2011, doi:10.1175/1520-0442(1993)006,1993:IVOTTC.2.0.CO;2.

Drevillon, M., C. Cassou, and L. Terray (2003), Model study of the North Atlantic region atmospheric response to autumn tropical Atlantic sea-surface-temperature anomalies, *Q. J. R. Meteorol. Soc.*, *129*, 2591–2611, doi:10.1256/qj.02.17.

Eden, C., and J. Willebrand (2001), Mechanism of interannual to decadal variability of the North Atlantic Circulation, *J. Clim.*, *14*, 2266–2280.

Enfield, D. B., A. M. Mestas-Nuñez, and P. J. Trimble (2001), The Atlantic multidecadal oscillation and its relation to rainfall and river flows in the continental U.S, *Geophys. Res. Lett.*, *28*, 2077–2080, doi:10.1029/2000GL012745.

Francis J. A., and S. J. Vavrus (2015) Evidence for a wavier jet stream in response to rapid Arctic warming. *Environ. Res. Lett.*, *10*, doi:10.1088/1748-9326/10/1/014005.

Gastineau, G., and C. Frankignoul (2015), Influence of the north Atlantic SST variability on the atmospheric circulation during the twentieth century, *J. Clim.*, *28*, 1396–1416.

Gastineau G., F. D'Andrea and C. Frankignoul (2013) Atmospheric response to the North Atlantic Ocean variability on seasonal to decadal time scales. *Clim. Dyn.*, *40*(9–10), 2311–2330.
Gray, S. T., L. J. Graumlich, J. L. Betancourt, and G. T. Pederson (2004), A tree-ring based reconstruction of the Atlantic Multidecadal Oscillation since 1567 A.D, *Geophys. Res. Lett.*, *31*, L12205, doi:10.1029/2004GL019932.
Gulev, S. K., M. Latif, N. Keenlyside, W. Park, and K. P. Koltermann (2013), North Atlantic Ocean control on surface heat flux on multidecadal timescales, *Nature*, *499*, 464–467.
Häkkinen, S., P. B. Rhines, and D. L. Worthen (2011), Atmospheric blocking and Atlantic multidecadal ocean variability, *Science*, *334*, 655–659.
Hodson, D. L. R., R. T. Sutton, C. Cassou, N. Keenlyside, Y. Okumura, and T. J. Zhou (2010), Climate impacts of recent multidecadal changes in Atlantic Ocean sea surface temperature: A multimodel comparison, *Clim. Dyn.*, *34*, 1041–58.
Hoskins, B. J., and D. J. Karoly (1981), The steady linear response of a spherical atmosphere to thermal and orographic forcing, *J. Atmos. Sci.*, *38*, 1179–1196.
Hoskins, B. J., I. N. James, and G. H. White (1983), The shape, propagation and mean-flow interaction of large-scale weather systems, *J. Atmos. Sci.*, *40*, 1595–1612.
Hurrell, J., and W. H. van Loon (1997), Decadal variations in climate associated with the North Atlantic Oscillation, *Clim. Change*, *36*, 301–326.
Hurrell, J. W., Y. Kushnir, G. Ottersen, and M. Visbeck (2003), An overview of the North Atlantic Oscillation, *Geophys. Monogr.-Ame. Geophys. Union*, *134*, 1–36.
Kay, J. E., et al. (2015), *The Community Earth System Model (CESM) Large Ensemble Project: A Community Resource for Studying Climate Change in the Presence of Internal Climate Variability*, *Bull. Am. Meteorol. Soc.*, doi:10.1175/BAMS-D-13-00255.1, in press.
Keenlyside, N. S., M. Latif, J. Jungclaus, L. Kornblueh, and E. Roeckner (2008), Advancing decadal-scale climate prediction in the North Atlantic sector, *Nature*, *453*, 84–88, doi:10.1038/nature06921.
Kerr, R. A. (2000), A North Atlantic climate pacemaker for the centuries, *Science*, *288*(5473), 1984–1986.
Knight, J. R. (2009), The Atlantic multidecadal oscillation inferred from the forced climate response in coupled general circulation models, *J. Clim.*, *22*, 1610–1625.
Knight, J. R., R. J. Allan, C. K. Folland, M. Vellinga, and M. E. Mann (2005), A signature of persistent natural thermohaline circulation cycles in observed climate, *Geophys. Res. Lett.*, *32*, L20708, doi:10.1029/2005GL024233.
Knight, J. R., C. K. Folland, and A. A. Scaife (2006), Climate impacts of the Atlantic Multidecadal Oscillation, *Geophys. Res. Lett.*, *33*, L17706, doi:10.1029/2006GL026242.
Knudsen, M. F., M.-S. Seidenkrantz, B. H. Jacobsen, and A. Kuijpers (2011), Tracking the Atlantic multidecadal oscillation through the last 8000 years, *Nat. Commun.*, *2*, 178, doi:10.1038/ncomms1186.
Knudsen, M. F., B. H. Jacobsen, M.-S. Seidenkrantz, and J. Olsen (2014), Evidence for external forcing of the Atlantic Multidecadal Oscillation since termination of the Little Ice Age, *Nat. Commun.*, *5*, 3323, doi:10.1038/ncomms4323.
Kuhlbrodt, T., A. Griesel, M. Montoya, A. Levermann, M. Hofmann, and S. Rahmstorf (2007), On the driving processes of the Atlantic meridional overturning circulation, *Rev. Geophys.*, *45*, RG2001, doi:10.1029/2004RG000166.
Kushnir, Y. (1994), Interdecadal variations in North-Atlantic sea-surface temperature and associated atmospheric conditions, *J. Clim.*, *7*, 141–157.
Lean, J. L., and D. H. Rind (2008), How natural and anthropogenic influences alter global and regional surface temperatures: 1889 to 2006, *Geophys. Res. Lett.*, *35*, L18701, doi:10.1029/2008GL034864.
Mahajan, S., R. Zhang, and T. L. Delworth (2011), Impact of the Atlantic Meridional Overturning Circulation (AMOC) on Arctic surface air temperature and sea ice variability, *J. Clim.*, *24*, 6573–6581.
Medhaug, I., and T. Furevik (2011), North Atlantic 20th century multidecadal variability in coupled climate models: Sea surface temperature and ocean overturning circulation, *Ocean Sci.*, *7*, 389–404.
Medhaug, I., H. R. Langehaug, T. Eldevik, T. Furevik, and M. Bentsen (2012), Mechanisms for decadal scale variability in a simulated Atlantic meridional overturning circulation, *Clim. Dyn.*, *39*, 77–93.
Meehl, G. A., et al. (2014), Decadal climate prediction: An update from the trenches, *Bull. Am. Meteorol. Soc.*, *95*, 243–267, doi:10.1175/BAMS-D-12-00241.1.
Michelangeli, P.-A., R. Vautard, and B. Legras (1995), Weather regimes: Recurrence and quasi stationarity, *J. Atmos. Sci.*, *52*, 1237–1256, doi:10.1175/1520-0469(1995)052<1237:WRRAQS>2.0.CO;2.
Minobe, S., A. Kuwano-Yoshida, N. Komori, S.-P. Xie, and R. J. Small (2008), Influence of the Gulf Stream on the troposphere, *Nature*, *452*, 206–209.
Mori, M., M. Watanabe, H. Shiogama, J. Inoue, and M. Kimoto (2014), Robust Arctic sea-ice influence on the frequent Eurasian cold winters in past decades, *Nat. Geosci.*, *7*, 869–873, doi:10.1038/NGEO2277.
Msadek, R., C. Frankignoul, K. W. Dixon, T. L. Delworth, and W. Hurlin (2010), Assessing the predictability of the Atlantic meridional overturning circulation and associated fingerprints, *Geophys. Res. Lett.*, *37*, L19608, doi:10.1029/2010GL044517.
Msadek, R., C. Frankignoul, and L. Li (2011), Mechanisms of the atmospheric response to North Atlantic multidecadal variability: A model study, *Clim. Dyn.*, *36*, 1255–1276.
Msadek, R., et al. (2014), Predicting a decadal shift in north Atlantic climate variability using the GFDL forecast system, *J. Clim.*, *27*, doi:10.1175/JCLI-D-13-00476.1.
Muir, L. C., and A. V. Fedorov (2015), How the AMOC affects ocean temperatures on decadal to centennial timescales: The North Atlantic versus an interhemispheric seesaw, *Clim. Dyn.*, *45*, 151–160.
Nakamura, H., T. Sampe, A. Goto, W. Ohfuchi, and S.-P. Xie (2008), On the importance of midlatitude oceanic frontal zones for the mean state and dominant variability in the tropospheric circulation, *Geophys. Res. Lett.*, *35*, L15709, doi:10.1029/2008GL034010.
Okumura, Y., S. P. Xie, A. Numaguti, and Y. Tanimoto (2001), Tropical Atlantic air-sea interaction and its influence on the NAO, *Geophys. Res. Lett.*, *28*, 1507–1510, doi:10.1029/2000GL012565.
Omrani, N. E., N. S. Keenlyside, J. R. Bader, and E. Manzini (2014), Stratosphere key for wintertime atmospheric response to warm Atlantic decadal conditions, *Clim. Dyn.*, *42*, 649–663.
Omrani, N.-E., J. Bader, N. S. Keenlyside, and E. Manzini (2015), Troposphere–stratosphere response to large-scale North Atlantic Ocean variability in an atmosphere/ocean coupled model, *Clim. Dyn.*, doi:10.1007/s00382-015-2654-6.
Otterå, O. H., M. Bentsen, H. Drange, and L. Suo (2010), External forcing as a metronome for Atlantic multidecadal variability, *Nat. Geosci.*, *3*, 688–694.
Overland, J., J. Francis, R. Hall, E. Hanna, S.-J. Kim, and T. Vihma (2015), The melting arctic and mid-latitude weather patterns: Are they connected? *J. Clim.*, doi:10.1175/JCLI-D-14-00822.1.
Peings, Y., and G. Magnusdottir (2014), Forcing of the wintertime atmospheric circulation by the multidecadal fluctuations of the North Atlantic Ocean, *Environ. Res. Lett.*, *9*(3), 034018, doi:10.1088/1748-9326/9/3/034018.

Peings, Y., and G. Magnusdottir (2015), Wintertime atmospheric response to Atlantic multidecadal variability: Effect of stratospheric representation and ocean–atmosphere coupling, *Clim. Dyn.*, doi:10.1007/s00382-015-2887-4.

Peng, S., W. A. Robinson, S. Li, and M. P. Hoerling (2005), Tropical Atlantic SST forcing of coupled North Atlantic seasonal responses, *J. Clim.*, *18*, 480–496, doi:10.1175/JCLI-3270.1.

Penland, C., and L. M. Hartten (2014), Stochastic forcing of north tropical Atlantic sea surface temperatures by the North Atlantic Oscillation, *Geophys. Res. Lett.*, *41*, 2126–2132, doi:10.1002/2014GL059252.

Rayner N. A., D. E. Parker, E. B. Horton, C. K. Folland, L. V. Alexander, D. P. Rowell, E. C. Kent, and A. Kaplan (2003) Global analyses of sea surface temperature, sea ice, and night marine air temperature since the late nineteenth century *J. Geophys. Res.*, *108*(D14), 4407, doi:10.1029/2002JD002670.

Rodwell, M. J., and D. P. Folland (2002), Atlantic air-sea interaction and seasonal predictability, *Q. J. R. Meteorol. Soc.*, *128*, 1413–1443.

Ruprich-Robert, Y., and C. Cassou (2014), Combined influences of seasonal East Atlantic Pattern and North Atlantic Oscillation to excite Atlantic multidecadal variability in a climate model, *Clim. Dyn.*, *44*, 229–253, doi:10.1007/s00382-014-2176-7.

Sato, K., J. Inoue, and M. Watanabe (2014), Influence of the Gulf Stream on the Barents Sea ice retreat and Eurasian coldness during early winter, *Environ. Res. Lett.*, *9*, 084009.

Smirnov, D., and D. J. Vimont (2012), Extratropical forcing of tropical Atlantic variability during boreal summer and fall, *J. Clim.*, *25*, 2056–2076.

Steinman, B. A., M. E. Mann, and S. K. Miller (2015), Atlantic and Pacific multidecadal oscillations and Northern Hemisphere temperatures, *Science*, doi:10.1126/science.1257856.

Sutton, R. T., and D. L. R. Hodson (2007), Climate response to basin-scale warming and cooling of the North Atlantic Ocean, *J. Clim.*, *20*, 891–907, doi:10.1175/JCLI4038.1.

Tandon, N. F., and P. J. Kushner (2015), Does external forcing interfere with the AMOC's influence on north Atlantic Sea surface temperature? *J. Clim.*, *28*, 6309–6323.

Terray, L. (2012), Evidence for multiple drivers of North Atlantic multi-decadal climate variability, *Geophys. Res. Lett.*, *39*, L19712, doi:10.1029/2012GL053046.

Terray, L., and C. Cassou (2002), Tropical Atlantic sea surface temperature forcing of quasi-decadal climate variability over the north Atlantic–European region, *J. Clim.*, *15*, 3170–3187.

Ting, M., Y. Kushnir, R. Seager, and C. Li (2009), Forced and internal twentieth-century SST in the North Atlantic, *J. Clim.*, *22*, 1469–1481.

Ting, M., Y. Kushnir, R. Seager, and C. Li (2011), Robust features of Atlantic multi-decadal variability and its climate impacts, *Geophys. Res. Lett.*, *38*, L17705, doi:10.1029/2011GL048712.

Ting, M., Y. Kushnir, and C. Li (2014), North Atlantic Multidecadal SST Oscillation: External forcing versus internal variability, *J. Mar. Syst.*, *133*, 27–38.

Trenberth, K. E., and D. J. Shea (2006), Atlantic hurricanes and natural variability in 2005, *Geophys. Res. Lett.*, *33*, L12704, doi:10.1029/2006GL026894.

Visbeck, M., H. Cullen, G. Krahmann, and N. Naik (1998), Ocean model's response to North Atlantic Oscillation-like wind forcing, *Geophys. Res. Lett.*, *25*, 4521–4524, doi:10.1029/1998GL900162.

Wallace, J. M., I. M. Held, D. W. J. Thompson, K. E. Trenberth, and J. E. Walsh (2014), Global warming and winter weather, *Science*, *343*(6172), 729–730, doi:10.1126/science.343.6172.729.

Woollings, T., C. Franzke, D. Hodson, B. Dong, E. Barnes, C. C. Raible, and J. Pinto (2015), Contrasting interannual and multidecadal NAO variability, *Clim. Dyn.*, *45*, 539–556.

Yeager, S. G., and G. Danabasoglu (2014), The origins of late-twentieth-century variations in the large-scale North Atlantic circulation, *J. Clim.*, *27*, 3222–3247, doi:10.1175/JCLI-D-13-00125.1.

Yeager, S. G., A. Karspeck, G. Danabasoglu, J. Tribbia, and H. Teng (2012), A decadal prediction case study: Late twentieth-century North Atlantic Ocean heat content, *J. Clim.*, *25*, 5173–5189, doi:10.1175/JCLI-D-11-00595.1.

Yeager, S. G., A. R. Karspeck, and G. Danabasoglu (2015), Predicted slowdown in the rate of Atlantic sea ice loss, *Geophys. Res. Lett.*, *42*, 10,704–10,713, doi:10.1002/2015GL065364.

Yu, B., G. J. Boer, F. W. Zwiers, and W. J. Merryfield (2011), Covariability of SST and surface heat fluxes in reanalyses and CMIP3 climate models, *Clim. Dyn.*, *36*, 589–605.

Zhang, L., and C. Wang (2013), Multidecadal North Atlantic sea surface temperature and Atlantic meridional overturning circulation variability in CMIP5 historical simulation, *J. Geophys. Res. Oceans*, *118*, 5772–5791, doi:10.1002/jgrc.20390.

Zhang, R. (2015), Mechanisms for low-frequency variability of summer Arctic sea ice extent, *Proc. Natl. Acad. Sci. U.S.A.*, *112*(15), 4570–4575, doi:10.1073/pnas.1422296112.

Zhang, R., and T. L. Delworth (2006), Impact of Atlantic multidecadal oscillations on India/Sahel rainfall and Atlantic hurricanes, *Geophys. Res. Lett.*, *33*, L17712, doi:10.1029/2006GL026267.

Zhang, R., et al. (2013), Have aerosols caused the observed Atlantic multidecadal variability? *J. Atmos. Sci.*, *70*, 1135–1144.